

Exclusive photoproduction of heavy quarkonia pairs

Sebastián Andradé[✉], Marat Siddikov[✉], and Iván Schmidt[✉]

*Departamento de Física, Universidad Técnica Federico Santa María,
y Centro Científico - Tecnológico de Valparaíso, Casilla 110-V, Valparaíso, Chile*

 (Received 10 February 2022; accepted 30 March 2022; published 29 April 2022)

In this paper we study the high-energy exclusive photoproduction of heavy quarkonia pairs in the leading order of the strong coupling constant α_s . In the suggested mechanism, the quarkonia pairs are produced with opposite charge parities, and predominantly have oppositely directed transverse momenta. Using the Color Glass Condensate approach, we numerically estimate the production cross sections in the kinematics of the forthcoming electron-proton colliders, as well as proton-ion colliders in ultraperipheral collisions. We find that the cross sections are within the reach of planned experiments and can be measured with reasonable precision. The suggested mechanism has a significantly larger cross section than that of the same C -parity quarkonia pair production.

DOI: [10.1103/PhysRevD.105.076022](https://doi.org/10.1103/PhysRevD.105.076022)

I. INTRODUCTION

The production of heavy quarkonia is frequently considered as a clean probe for the study of gluon dynamics in high-energy interactions, since in the limit of heavy quark mass m_Q the running coupling becomes small, and it is possible to apply perturbative methods for the description of quark-gluon interactions. In many scattering problems the small size of the color-singlet heavy quarkonium provides additional twist suppression [1,2], thus facilitating the applicability of perturbative treatments. The modern nonrelativistic QCD framework allows to use quarkonia production as a powerful probe of strong interactions, systematically taking into account various perturbative corrections [3–14].

For precision studies of hadronic interactions, *exclusive* production presents a special interest in view of its simpler structure. However, up to now most of the experimental data on exclusive heavy quarkonia production were limited to channels with single quarkonia in the final state. This limitation was largely motivated by probable smaller cross sections of events with more than one quarkonia in the final state. Nevertheless, processes with two mesons in the final state are particularly interesting and have been the subject of studies since the early days of QCD [15–18]. A recent discovery of all-heavy tetraquarks, which might be considered as molecular states of two quarkonia, has

significantly reinvigorated interest in the study of this channel [19–29].

In LHC kinematics most of the previous studies of exclusive double quarkonia production [30–35] focused on the so-called two-photon mechanism, $\gamma\gamma \rightarrow M_1 M_2$, which gives the dominant contribution for the production of quarkonia pairs with the same C parity in ultraperipheral collisions. Studies beyond the double-photon fusion show that, in a transverse momentum distribution factorization approach, the exclusive double quarkonia production could allow to measure the currently unknown generalized transverse momentum distributions of gluons [36]. However, in LHC kinematics the cross section of this process can get sizable contributions from the so-called multiparton scattering diagrams. Such contributions depend on the poorly known multigluon distributions, leading to potential ambiguities in the theoretical interpretation of the data.

Electron-proton collisions have a significant advantage for studies of heavy quarkonia pair production, due to a smaller number of production mechanisms compared to hadron-hadron collisions. Moreover, precision studies of double quarkonia production in ep collisions could become possible after the launch of new high-luminosity facilities, such as the forthcoming Electron-Ion Collider (EIC) [37–40], the future Large Hadron electron Collider (LHeC) [41], the Future Circular Collider (FCC-he) [42–44], and the CEPC collider [45,46]. The main objective of this manuscript is the study of exclusive production of heavy quarkonia pairs, $\gamma p \rightarrow M_1 M_2 p$, in the kinematics of the above-mentioned electron-proton colliders. Potentially, such production might also be probed in ultraperipheral heavy-ion and proton-ion collisions.

Published by the American Physical Society under the terms of the Creative Commons Attribution 4.0 International license. Further distribution of this work must maintain attribution to the author(s) and the published article's title, journal citation, and DOI. Funded by SCOAP³.

However, in these cases the analysis becomes more complicated in view of possible contributions of other mechanisms [30–34]. The large mass m_q of the heavy flavors justifies the perturbative treatment in a wide kinematic range, without additional restrictions on the virtuality of the incoming photon Q^2 or the invariant mass of the produced quarkonia pair. In the absence of imposed kinematic constraints, the dominant contribution to the cross section will come from events induced by quasireal photons with small $Q^2 \approx 0$ and relatively small values of $x_B \ll 1$. In this kinematics it is appropriate to use the language of color dipole amplitudes and apply the color dipole (also known as Color Glass Condensate or CGC) framework [47–55]. At high energies the color dipoles are eigenstates of interaction, and thus can be used as universal elementary building blocks, automatically accumulating both the hard and soft fluctuations [56]. The light-cone color dipole framework has been developed and successfully applied to the phenomenological description of both hadron-hadron and lepton-hadron collisions [57–64], and for this reason we will use it for our estimates.

The paper is structured as follows. In Sec. II we theoretically evaluate the cross section of exclusive photoproduction of heavy quarkonia pairs in the CGC approach. In Sec. III we present our numerical estimates, in the kinematics of the future ep colliders (EIC, LHeC, and FCC-he) and ultraperipheral pA collisions at the LHC. Finally, in Sec. IV we draw conclusions.

II. EXCLUSIVE MESON PAIR PHOTOPRODUCTION

A. Kinematics of the process

We would like to start our discussion of the theoretical framework with a short description of the kinematics of the process. Our choice of the light-cone decomposition of particle momenta is similar to that of earlier studies of pion-pair [65–69] and single-meson production [70–86]. However, we should take into account that the mass of the quarkonium (in contrast to that of the pion) is quite large, and thus cannot be disregarded as a kinematic higher-twist correction. Besides, for photoproduction this mass can appear as one of the hard scales in the problem.

In what follows we will use the notations q for the photon momentum, P and P' for the momentum of the proton before and after the collision, and p_1, p_2 for the 4-momenta of produced heavy quarkonia. For sake of generality, we will assume temporarily that the photon can have a nonzero virtuality $-q^2 = Q^2$, taking later that for photoproduction $Q^2 = 0$. We will also use the notation Δ for the momentum transfer to the proton, $\Delta = P' - P$, and the notation t for its square, $t \equiv \Delta^2$. The light-cone

expansion of the above-mentioned momenta in the lab frame is given by¹

$$q = \left(q^+, \frac{Q^2}{2q^+}, \mathbf{0}_\perp \right), \quad q^+ = E_\gamma + \sqrt{E_\gamma^2 + Q^2} \approx 2E_\gamma, \quad (1)$$

$$P = \left(\frac{m_N^2}{2P^-}, P^-, \mathbf{0}_\perp \right), \quad P^- = E_p + \sqrt{E_p^2 - m_N^2} \approx 2E_p, \quad (2)$$

$$p_a = \left(M_a^\perp e^{y_a}, \frac{M_a^\perp e^{-y_a}}{2}, \mathbf{p}_a^\perp \right), \quad a = 1, 2, \quad (3)$$

$$M_a^\perp \equiv \sqrt{M_a^2 + (\mathbf{p}_a^\perp)^2}, \quad (4)$$

where $(y_a, \mathbf{p}_a^\perp)$ are the rapidity and transverse momentum of the quarkonium a , and M_a is its mass. Using conservation of 4-momentum, we may obtain for the momentum transfer to the proton

$$\begin{aligned} \Delta &= P' - P = q - p_1 - p_2 \\ &= \left(q^+ - M_1^\perp e^{y_1} - M_2^\perp e^{y_2}, \frac{Q^2}{2q^+} \right. \\ &\quad \left. - \frac{M_1^\perp e^{-y_1} + M_2^\perp e^{-y_2}}{2}, -\mathbf{p}_1^\perp - \mathbf{p}_2^\perp \right), \end{aligned} \quad (5)$$

and for the variable $t \equiv \Delta^2$,

$$\begin{aligned} t = \Delta^2 &= (q^+ - M_1^\perp e^{y_1} - M_2^\perp e^{y_2}) \left(\frac{Q^2}{q^+} - M_1^\perp e^{-y_1} - M_2^\perp e^{-y_2} \right) \\ &\quad - (\mathbf{p}_1^\perp + \mathbf{p}_2^\perp)^2. \end{aligned} \quad (6)$$

After the interaction, the 4-momentum of the proton is given by

$$\begin{aligned} P' &= P + \Delta = \left(q^+ + \frac{m_N^2}{2P^-} - M_1^\perp e^{y_1} - M_2^\perp e^{y_2}, \right. \\ &\quad \left. P^- + \frac{Q^2}{2q^+} - \frac{M_1^\perp e^{-y_1} + M_2^\perp e^{-y_2}}{2}, -\mathbf{p}_1^\perp - \mathbf{p}_2^\perp \right), \end{aligned} \quad (7)$$

and the on-shell-ness condition $(P + \Delta)^2 = m_N^2$ allows to get an additional constraint

¹In earlier theoretical studies [65–68,80,87] the evaluations were done in the so-called symmetric frame, in which the z axis is chosen in such a way that the vectors q and $\bar{P} \equiv P + P'$ do not have transverse components. Besides, all evaluations were done in the Bjorken limit, assuming an infinitely large Q^2 and negligibly small masses of the produced mesons (pions). In our studies we consider quasireal photons, with $Q^2 \approx 0$, and moreover the heavy mass of the quarkonia does not allow to drop certain “higher-twist” terms. For this reason, the kinematic expressions in the symmetric frame become quite complicated, and there is no advantage in its use for photoproduction.

$$q \cdot P \equiv q^+ P^- = P^- (M_1^\perp e^{y_1} + M_2^\perp e^{y_2}) - \frac{m_N^2 + t}{2} + \frac{m_N^2}{4P^-} \left(M_1^\perp e^{-y_1} + M_2^\perp e^{-y_2} - \frac{Q^2}{q^+} \right). \quad (8)$$

Solving Eq. (8) with respect to $q \cdot P$, we get

$$q \cdot P = \frac{P^- (M_1^\perp e^{y_1} + M_2^\perp e^{y_2}) - \frac{m_N^2 + t}{2} + \frac{m_N^2}{4P^-} (M_1^\perp e^{-y_1} + M_2^\perp e^{-y_2})}{2} \pm \frac{1}{2} \sqrt{\left(P^- (M_1^\perp e^{y_1} + M_2^\perp e^{y_2}) - \frac{m_N^2 + t}{2} + \frac{m_N^2}{4P^-} (M_1^\perp e^{-y_1} + M_2^\perp e^{-y_2}) \right)^2 + Q^2 m_N^2}, \quad (9)$$

which allows to express the energy of the photon $E_\gamma \approx q^+/2$ in terms of the kinematic variables $(y_a, \mathbf{p}_a^\perp)$ of the produced quarkonia. In the kinematics of all experiments that we consider below, the typical values $q^+, P^- \gg \{Q, M_a, m_N, \sqrt{t}\}$, and for this reason we may approximate Eq. (9) as

$$q \cdot P \equiv q^+ P^- \approx P^- (M_1^\perp e^{y_1} + M_2^\perp e^{y_2}), \quad \text{or} \quad (10)$$

$$q^+ \approx M_1^\perp e^{y_1} + M_2^\perp e^{y_2}. \quad (11)$$

From a comparison of Eqs. (3) and (8), we may see that at high energies the light-cone plus component of the photon momentum q^+ is shared between the momenta of the produced quarkonia, whereas the momentum transfer to the proton (vector Δ) has a negligibly small plus component, in agreement with the eikonal picture expectations. Equations (9)–(10) allow to express the Bjorken variable x_B , which appears in the analysis of this process in Bjorken kinematics, using its conventional definition $x_B = Q^2/2(p \cdot q) \approx Q^2/(Q^2 + W^2)$. As discussed in Refs. [88–91], in phenomenological studies it is usually assumed that for heavy quarks all the gluon densities and forward dipole amplitudes should depend on the so-called “rescaling variable”

$$x = x_B \left(1 + \frac{(4m_Q)^2}{Q^2} \right) = \frac{Q^2 + (4m_Q)^2}{2(p \cdot q)}, \quad (12)$$

which was introduced in Ref. [88] in order to improve the description of the near-threshold heavy quarkonia production. While the color dipole framework is usually applied far from the near-threshold kinematics, the use of the variable x instead of x_B for heavy quarks improves agreement of dipole-approach predictions with experimental data. In the Bjorken limit, the variable x coincides with x_B . For small $Q^2 \approx 0$ (photoproduction regime) the variable x_B vanishes, whereas x remains finite and is given by the approximate expression

$$x = \frac{Q^2 + (4m_Q)^2}{2(p \cdot q)} \Big|_{Q \approx 0} \approx \frac{8m_Q^2}{P^- (M_1^\perp e^{y_1} + M_2^\perp e^{y_2})} + \mathcal{O}\left(\frac{Q^2}{m_Q^2}\right) \approx \frac{4m_Q^2}{E_p (M_1^\perp e^{y_1} + M_2^\perp e^{y_2})}. \quad (13)$$

In this study, we are interested in the production of both quarkonia at central rapidities (in the lab frame) by high-energy photon-proton collisions. In this kinematics the variable x is very small, which suggests that the amplitude of this process should be analyzed in frameworks with built-in saturation, such as the CGC. In contrast, in the Bjorken limit ($Q^2 \rightarrow \infty, Q^2/2p \cdot q = \text{const}$) we observe that the variable x can be quite large, so it is more appropriate to analyze this kinematics using collinear or k_T factorization. The latter case requires a separate study and will be presented elsewhere.

In the photoproduction approximation the invariant energy of the γp collision can be written as

$$W^2 \equiv s_{\gamma p} = (q + P)^2 = -Q^2 + m_N^2 + 2q \cdot P \approx -m_N^2 + P^- (M_1^\perp e^{y_1} + M_2^\perp e^{y_2}), \quad (14)$$

whereas the invariant mass of the produced heavy quarkonia pair is given by

$$M_{12}^2 = (p_1 + p_2)^2 = M_1^2 + M_2^2 + 2(M_1^\perp M_2^\perp \cosh(y_1 - y_2) - \mathbf{p}_1^\perp \cdot \mathbf{p}_2^\perp). \quad (15)$$

In electron-proton collisions the cross section of heavy meson pairs is dominated by a single-photon exchange between its leptonic and hadronic parts, and for this reason can be represented as

$$\frac{d\sigma_{e p \rightarrow e M_1 M_2 p}}{dQ^2 dy_1 d^2 \mathbf{p}_1^\perp dy_2 d^2 \mathbf{p}_2^\perp} = \frac{\alpha_{\text{em}}}{\pi Q^2} \left[(1-y) \frac{d\sigma_L}{dy_1 d^2 \mathbf{p}_1^\perp dy_2 d^2 \mathbf{p}_2^\perp} + \left(1-y + \frac{y^2}{2} \right) \frac{d\sigma_T}{dy_1 d^2 \mathbf{p}_1^\perp dy_2 d^2 \mathbf{p}_2^\perp} \right], \quad (16)$$

where we use the standard deep inelastic scattering notation y for the elasticity (i.e., the fraction of electron energy that passes to the photon, not to be confused with the rapidities y_a of the produced quarkonia). The subscript letters L, T on the right-hand side of Eq. (16) stand for the contributions of longitudinally and transversely polarized photons, respectively. The structure of Eq. (16) suggests that the dominant contribution to the cross section comes from the region of small Q^2 . In this kinematics the contribution of $d\sigma_L$ is suppressed compared to the term $d\sigma_T$. This expectation is partially corroborated by the experimental data from ZEUS [92] and H1 [93], which found that for *single* quarkonia production in the region $Q^2 \lesssim 1 \text{ GeV}^2$ the longitudinal cross section $d\sigma_L$ constitutes less than 10% of the transverse cross section $d\sigma_T$. For this reason, in this paper we will disregard the cross section $d\sigma_L$ altogether, while the relevant cross section $d\sigma_T$ is

$$\frac{d\sigma_T}{dy_1 d|p_1^\perp|^2 dy_2 d|p_2^\perp|^2 d\phi} \approx \frac{1}{256\pi^4} |\mathcal{A}_{\gamma T p \rightarrow M_1 M_2 p}|^2 \delta\left(\frac{M_1^\perp e^{y_1} + M_2^\perp e^{y_2}}{q^+} - 1\right), \quad (17)$$

where $\mathcal{A}_{\gamma T p \rightarrow M_1 M_2 p}$ is the amplitude of the exclusive process, induced by a transversely polarized photon, and ϕ is the angle between the vectors \mathbf{p}_1 and \mathbf{p}_2 in the transverse plane. The δ function in Eq. (17) reflects the conservation of the plus component of momentum, discussed earlier in Eq. (8).

Similarly, for exclusive *hadro* production $pA \rightarrow pAM_1M_2$ in ultraperipheral kinematics we may obtain the cross section using the equivalent photon (Weizsäcker-Williams) approximation,

$$\frac{d\sigma(p + A \rightarrow p + A + M_1 + M_2)}{dy_1 d^2\mathbf{p}_1^\perp dy_2 d^2\mathbf{p}_2^\perp} = \int dn_\gamma(\omega \equiv E_\gamma, \mathbf{q}_\perp) \frac{d\sigma_T(\gamma + p \rightarrow \gamma + p + M_1 + M_2)}{dy_1 d^2\mathbf{p}_1^* dy_2 d^2\mathbf{p}_2^*}, \quad (18)$$

where $dn_\gamma(\omega \equiv E_\gamma, \mathbf{q}_\perp)$ is the spectral density of the flux of photons created by the nucleus, \mathbf{q}_\perp is the transverse momentum of the photon with respect to the nucleus, and the energy E_γ of the photon can be related to the kinematics of produced quarkonia using Eqs. (9)–(10). The explicit expression for $dn_\gamma(\omega \equiv E_\gamma, \mathbf{q}_\perp)$ can be found in Ref. [94]. The momenta $\mathbf{p}_i^* = \mathbf{p}_i^\perp - \mathbf{q}_\perp$ are the transverse parts of the quarkonia momenta with respect to the produced photon. Due to nuclear form factors, the typical values of momenta \mathbf{q}_\perp are controlled by the nuclear radius R_A and are quite small, $\langle \mathbf{q}_\perp^2 \rangle \sim \langle Q^2 \rangle \sim \langle R_A^2 \rangle^{-1} \lesssim (0.2 \text{ GeV}/A^{1/3})^2$. For this reason, for very heavy ions ($A \gg 1$) we may expect that the p_T dependence of the cross sections on the left-hand side of

Eq. (18) largely repeats the p_T dependence of the cross section in the integrand on the right-hand side. For the special and experimentally important case of the \mathbf{p}^\perp -integrated cross section, Eq. (18) simplifies and can be rewritten as

$$\frac{d\sigma(p + A \rightarrow p + A + M_1 + M_2)}{dy_1 dy_2} = \int dE_\gamma \frac{dN_\gamma(\omega \equiv E_\gamma)}{dE_\gamma} \frac{d\sigma_T(\gamma + p \rightarrow \gamma + p + M_1 + M_2)}{dy_1 dy_2}, \quad (19)$$

where

$$N_\gamma(\omega) \equiv \int d^2\mathbf{q}_\perp \frac{dn_\gamma(\omega, \mathbf{q}_\perp)}{d\omega d^2\mathbf{q}_\perp}. \quad (20)$$

In the following Sec. II B we evaluate the amplitude $\mathcal{A}_{\gamma T p \rightarrow M_1 M_2 p}$, which determines the cross sections of photo-production processes.

B. Amplitude of the process in the color dipole picture

Since the formation time of rapidly moving heavy quarkonia significantly exceeds the size of the proton, the quarkonia formation occurs far outside the interaction region. For this reason, the amplitudes of the quarkonia production processes can be represented as a convolution of the quarkonia wave functions with hard amplitudes, which characterize the production of the small pairs of nearly on-shell heavy quarks in the gluonic field of the target. In what follows, we will refer to these nearly on-shell quarks as “produced” or “final-state” quarks. For exclusive production the cross section falls rapidly as a function of the transverse momenta p_T of the produced quarkonia, and for this reason we expect that the quarkonia will be produced predominantly with small momenta. In this kinematical region it is possible to completely disregard the color-octet contributions [8,9]. As was shown in Refs. [89–91], this assumption gives a very good description of the exclusive production of *single* quarkonia.

The general rules for the evaluation of different hard amplitudes in terms of the color-singlet forward dipole amplitude were introduced in Refs. [47,49–55] and are briefly summarized in Appendix A. This approach is based on the high-energy eikonal picture, and therefore the parton’s transverse coordinates and helicities remain essentially frozen during propagation in the gluonic field of the target. The hard scale, which controls the interaction of a heavy quark with the strong gluonic field, is its mass m_Q , so in the heavy-mass limit we may treat this interaction perturbatively. However, the interaction of gluons with each other, as well as with light quarks, remains strongly nonperturbative in the deeply saturated regime.

In the leading order over the strong coupling $\alpha_s(m_Q)$, there are a few dozen Feynman diagrams that contribute to

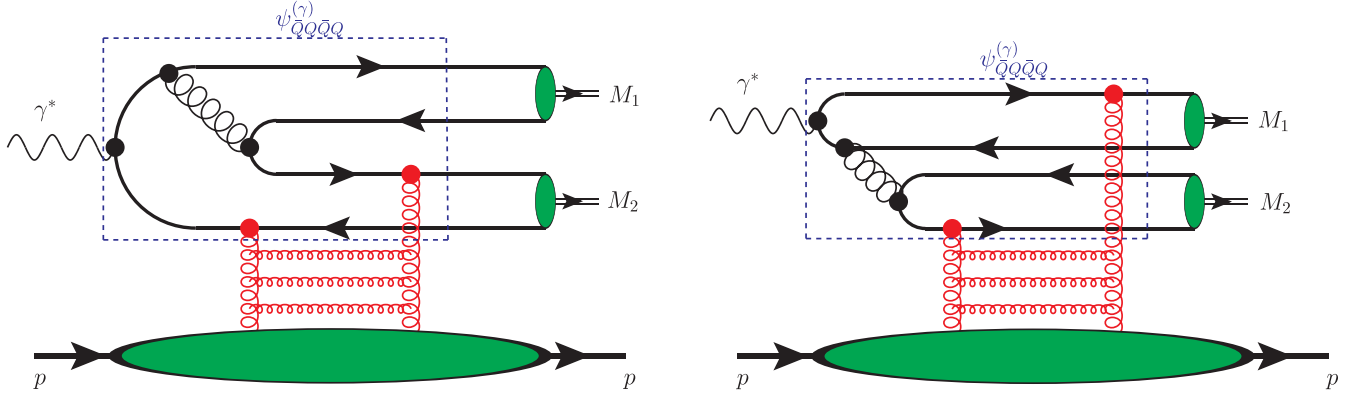


FIG. 1. Main classes of diagrams that contribute in the leading order over $\alpha_s(m_Q)$ to exclusive photoproduction of quarkonia pairs (type-A and type-B diagrams). The eikonal interactions are shown schematically as exchanges of t -channel gluons, indicated by the red wavy lines. In both plots, (a) summation over all possible attachments of t -channel gluons to partons in the upper part of diagram and (b) the inclusion of diagrams with inverted direction of heavy quark lines (“charge conjugation”) are implied. In the right diagram the t -channel gluons must be connected to different quark loops in order to guarantee a *color singlet* $\bar{Q}Q$ in the final state. The blue dashed rectangle schematically shows the part of the diagrams that (in the absence of eikonal interactions) contribute to the $\bar{Q}Q\bar{Q}Q$ component of the photon wave function $\psi_{\bar{Q}Q\bar{Q}Q}^{(\gamma)}$.

the exclusive photoproduction of meson pairs. In what follows, it is convenient to represent them as one of the two main classes shown schematically in Fig. 1. For the sake of definiteness, all the diagrams in which quarkonia are formed from different heavy quark lines (as shown in the left panel of Fig. 1) will be referred to as “type-A” diagrams. The opposite case, when quarkonia are formed from the same quark lines (as shown in the right panel of the Fig. 1), will be referred to as “type-B” diagrams. This classification is convenient for a discussion of symmetries, as well as for analysis of quarkonia production with mixed flavors. For example, production of $B_c^+ B_c^-$ pairs clearly gets contributions only from type-A diagrams, whereas production of mixed-flavor hidden-charm and hidden-bottom quarkonia (e.g., $J/\psi + \eta_b$) gets contributions only from type-B diagrams.

In configuration space the eikonal interactions with the target do not affect the impact parameters of the partons, so the interaction basically reduces to a mere multiplication of target-dependent factors, as discussed in Appendix A. This allows to express the amplitude of the whole process as a convolution of the four-quark Fock component wave function $\psi_{\bar{Q}Q\bar{Q}Q}^{(\gamma)}$ of the photon with dipole amplitudes and wave functions of the produced quarkonia. The amplitude of the process $\gamma^* p \rightarrow M_1 M_2 p$ can be represented as a sum,

$$\mathcal{A}(y_1, \mathbf{p}_1^\perp, y_2, \mathbf{p}_2^\perp) = \mathcal{A}_1(y_1, \mathbf{p}_1^\perp, y_2, \mathbf{p}_2^\perp) + \mathcal{A}_2(y_1, \mathbf{p}_1^\perp, y_2, \mathbf{p}_2^\perp), \quad (21)$$

where \mathcal{A}_1 and \mathcal{A}_2 stand for contributions of all type-A and type-B diagrams. Explicitly, these amplitudes are given by

$$\begin{aligned} \mathcal{A}_1(y_1, \mathbf{p}_1^\perp, y_2, \mathbf{p}_2^\perp) &= \prod_{i=1}^4 \left(\int d\alpha_i d^2 \mathbf{x}_i \right) \delta \left(\sum_k \alpha_k - 1 \right) \sum_{\ell n} \tilde{\sigma}_\ell \sigma_n c_{\ell n} \gamma(\mathbf{b}_\ell) \gamma(\mathbf{b}_n) \\ &\times [\Psi_{M_1}^\dagger(\alpha_{14}, \mathbf{r}_{14}) \Psi_{M_2}^\dagger(\alpha_{23}, \mathbf{r}_{23}) e^{i(\mathbf{p}_1^\perp \cdot \mathbf{b}_{14} + \mathbf{p}_2^\perp \cdot \mathbf{b}_{23})} \delta(y_1 - \mathcal{Y}_{14}) \delta(y_2 - \mathcal{Y}_{23}) \\ &+ \Psi_{M_1}^\dagger(\alpha_{23}, \mathbf{r}_{23}) \Psi_{M_2}^\dagger(\alpha_{14}, \mathbf{r}_{14}) e^{i(\mathbf{p}_1^\perp \cdot \mathbf{b}_{23} + \mathbf{p}_2^\perp \cdot \mathbf{b}_{14})} \delta(y_1 - \mathcal{Y}_{23}) \delta(y_2 - \mathcal{Y}_{14})] \\ &\times \psi_{\bar{Q}Q\bar{Q}Q}^{(\gamma)}(\alpha_1, \mathbf{x}_1; \alpha_2, \mathbf{x}_2; \alpha_3, \mathbf{x}_3; \alpha_4, \mathbf{x}_4; q), \end{aligned} \quad (22)$$

$$\begin{aligned} \mathcal{A}_2(y_1, \mathbf{p}_1^\perp, y_2, \mathbf{p}_2^\perp) &= \prod_{i=1}^4 \left(\int d\alpha_i d^2 \mathbf{x}_i \right) \delta \left(\sum_k \alpha_k - 1 \right) \sum_{\ell n} \tilde{\sigma}_\ell \sigma_n c_{\ell n} \gamma(\mathbf{b}_\ell) \gamma(\mathbf{b}_n) \\ &\times [\Psi_{M_1}^\dagger(\alpha_{12}, \mathbf{r}_{12}) \Psi_{M_2}^\dagger(\alpha_{34}, \mathbf{r}_{34}) e^{i(\mathbf{p}_1^\perp \cdot \mathbf{b}_{12} + \mathbf{p}_2^\perp \cdot \mathbf{b}_{34})} \delta(y_1 - \mathcal{Y}_{12}) \delta(y_2 - \mathcal{Y}_{34}) \\ &+ \Psi_{M_1}^\dagger(\alpha_{34}, \mathbf{r}_{34}) \Psi_{M_2}^\dagger(\alpha_{12}, \mathbf{r}_{12}) e^{i(\mathbf{p}_1^\perp \cdot \mathbf{b}_{34} + \mathbf{p}_2^\perp \cdot \mathbf{b}_{12})} \delta(y_1 - \mathcal{Y}_{34}) \delta(y_2 - \mathcal{Y}_{12})] \\ &\times \psi_{\gamma^* \rightarrow \bar{Q}Q\bar{Q}Q}(\alpha_1, \mathbf{x}_1; \alpha_2, \mathbf{x}_2; \alpha_3, \mathbf{x}_3; \alpha_4, \mathbf{x}_4; q), \end{aligned} \quad (23)$$

where we introduced a few shorthand notations, which characterize the pair of heavy partons i and j : the relative distance between them $\mathbf{r}_{ij} = \mathbf{x}_i - \mathbf{x}_j$, the light-cone fraction $\alpha_{ij} = \alpha_i/(\alpha_i + \alpha_j)$ carried by the quark in the pair (ij), and the transverse coordinate of its center of mass $\mathbf{b}_{ij} = (\alpha_i \mathbf{x}_i + \alpha_j \mathbf{x}_j)/(\alpha_i + \alpha_j)$. The notation $\sum_{\ell n}$ in the first line of Eqs. (22) and (23) implies summation over all possible attachments of t -channel gluons to the partons in the upper part of the diagram. For type- A diagrams the variables ℓ, n may independently take six different values, which correspond to connections to final quarks, a virtual quark, or a virtual gluon. For type- B diagrams both produced quark pairs must be in a color-singlet state, which translates into the additional constraint that ℓ, n should be connected to *different* quark loops (either upper or lower quark-antiquark pairs). The factors σ_ℓ, σ_n in the first line of Eqs. (22) and (23) have the value $+1$ if the corresponding t -channel gluon is connected to a quark line or gluon, and -1 otherwise. On the other hand, the color factors $c_{\ell n}$ depend on the topology of the diagram under consideration, that is, *how* the t -channel gluons are connected to the quark lines. For type- A diagrams, the color factor $c_{\ell n} = \mathcal{C}_1 \equiv \frac{1}{N_c^2 - 1} \text{tr}_c(t_a t_a t_b t_b) = (N_c^2 - 1)/4N_c$ if both t -channel gluons are connected to the same quark line or quark and antiquark lines of opposite color (e.g., quark-antiquark lines originating from a colorless photon or leading to the formation of colorless quarkonium). If the vertices of the t -channel gluons are separated by a color-changing vertex of a virtual gluon, then the color factor is given by $c_{\ell n} = \mathcal{C}_2 \equiv \frac{1}{N_c^2 - 1} \text{tr}_c(t_a t_b t_a t_b) = -1/4N_c$. For the diagrams with one three-gluon vertex, when one of the t -channel gluons is attached to a virtual gluon, the corresponding color factor is

$c_{\ell n} = \pm \mathcal{C}_3 = \pm N_c/4$, where the sign is positive for the diagram with attachment of the other t -channel gluon to the upper quark-antiquark pair (i.e., partons 1,2), and negative otherwise. Finally, for the diagram when both t -channel gluons are attached to a virtual (intermediate) gluon, the corresponding factor is $c_{\ell n} = \mathcal{C}_4 \equiv N_c/2$. For type- B diagrams, the corresponding color factor is $c_{\ell n} = \frac{1}{N_c^2 - 1} [\text{tr}_c(t_a t_c)]^2 = \frac{1}{4}$ for all possible connections of t -channel gluons. The functions $\gamma(\dots)$ characterize the interaction of the parton with the target and can be related to the dipole amplitude, as explained in Appendix A. The variables $\mathbf{b}_\ell, \mathbf{b}_n$ in the arguments of $\gamma(\dots)$ functions stand for the transverse coordinate of the parton that interacts with a t -channel gluon. For the final quarks this variable corresponds to the transverse coordinates of these partons (the integration variables \mathbf{x}_i). For intermediate partons this variable is the position of the center of mass of all final quarks that are produced at later stages,

$$\mathbf{b}_{j_1 \dots j_n} = \frac{\sum_{j=j_1 \dots j_n} \alpha_j \mathbf{x}_j}{\sum_{j=j_1 \dots j_n} \alpha_j}, \quad (24)$$

where the summation is done over all final quarks j_1, \dots, j_n that stem from a given parton. The notations Ψ_{M_1}, Ψ_{M_2} are used for the wave functions of the final-state quarkonia M_1 and M_2 (for the moment we completely disregard their spin indices), and $\psi_{\bar{Q}Q\bar{Q}Q}^{(\gamma)}(\{\alpha_i, \mathbf{x}_i\}; q)$ is the four-quark light-cone wave function of the virtual photon γ^* , which is evaluated in Appendix B 2. The product $\sum_{\ell n} \sigma_\ell \sigma_n c_{\ell n} \gamma(\mathbf{b}_\ell) \gamma(\mathbf{b}_n)$ can be expressed as a linear superposition of the color-singlet dipole amplitudes $N(x, \mathbf{r}_{ij}, \mathbf{b}_{ij})$ (see derivation in Appendix C). For the type- A contribution, the final result is

$$\begin{aligned} \sum_{\ell n} \sigma_\ell \sigma_n c_{\ell n} \gamma(\mathbf{b}_\ell) \gamma(\mathbf{b}_n) = & \left\{ \frac{2 - N_c^2}{4N_c} N(x, \mathbf{r}_{14}, \mathbf{b}_{14}) - \frac{1}{2N_c} N(x, \mathbf{r}_{34}, \mathbf{b}_{34}) - \frac{3 + 5N_c^2}{4N_c} N(x, \mathbf{r}_{12}, \mathbf{b}_{12}) \right. \\ & + \frac{1}{4N_c} \left[N(x, \mathbf{r}_{23}, \mathbf{b}_{23}) - N\left(x, \frac{\alpha_1 \mathbf{r}_{14} + \alpha_3 \mathbf{r}_{34}}{1 - \alpha_2}, \mathbf{b}_{1344}\right) \right] \\ & + \frac{N_c^2 + 2}{4N_c} N(x, \mathbf{r}_{13}, \mathbf{b}_{13}) + \frac{3N_c^2 - 2}{4N_c} N\left(x, \frac{\alpha_1 \mathbf{r}_{21} + \alpha_3 \mathbf{r}_{23} + \alpha_4 \mathbf{r}_{24}}{1 - \alpha_2}, \mathbf{b}_{1234}\right) \\ & + \frac{3N_c}{2} N\left(x, \frac{\alpha_3 \mathbf{r}_{13} + \alpha_4 \mathbf{r}_{14}}{\alpha_3 + \alpha_4}, \mathbf{b}_{134}\right) + 2N_c N\left(x, \frac{\alpha_3 \mathbf{r}_{23} + \alpha_4 \mathbf{r}_{24}}{\alpha_3 + \alpha_4}, \mathbf{b}_{234}\right) \\ & + \frac{N_c^2 + 1}{4N_c} \left[N\left(x, \frac{\alpha_3 \mathbf{r}_{13} + \alpha_4 \mathbf{r}_{14}}{1 - \alpha_2}, \mathbf{b}_{1134}\right) + N(x, \mathbf{r}_{24}, \mathbf{b}_{24}) \right] \\ & - \frac{N_c}{2} \left[N\left(x, \frac{\alpha_4 \mathbf{r}_{34}}{\alpha_3 + \alpha_4}, \mathbf{b}_{334}\right) + N\left(x, -\frac{\alpha_3 \mathbf{r}_{34}}{\alpha_3 + \alpha_4}, \mathbf{b}_{344}\right) \right] \\ & - \frac{N_c}{2} N\left(x, -\frac{\alpha_1(\alpha_3 \mathbf{r}_{13} + \alpha_4 \mathbf{r}_{14})}{(\alpha_3 + \alpha_4)(\alpha_1 + \alpha_3 + \alpha_4)}, \mathbf{b}_{34,134}\right) \\ & \left. - \frac{N_c^2 - 1}{4N_c} N\left(x, \frac{\alpha_1 \mathbf{r}_{31} + \alpha_4 \mathbf{r}_{34}}{1 - \alpha_2}, \mathbf{b}_{1334}\right) \right\}, \quad (25) \end{aligned}$$

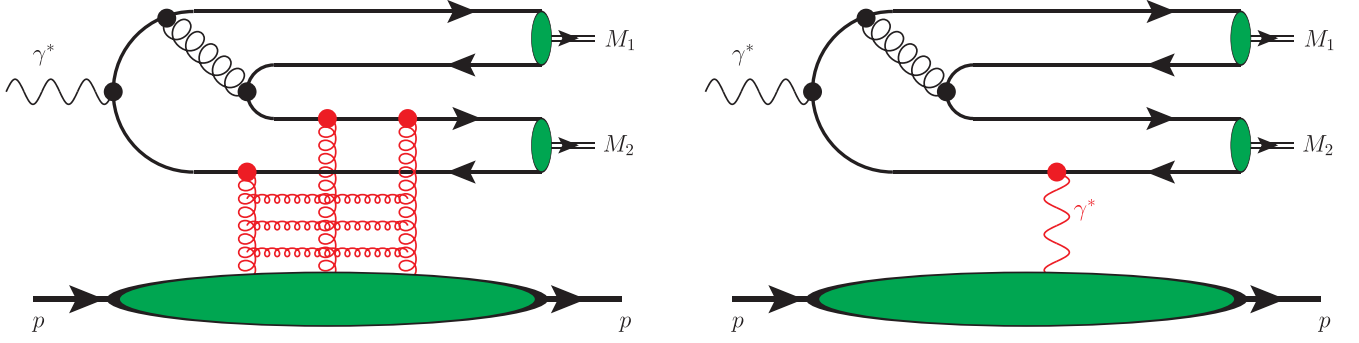


FIG. 2. Examples of higher-order contributions, which become relevant for the exclusive production of quarkonia with the same C parity. The left diagram corresponds to the exchange of an odderon (three-gluon ladder) in the t channel, whereas the right diagram corresponds to photon exchange in the t channel. In both plots summation is implied over summation over all possible attachments of t -channel gluons and photon (red) to black-colored partonic lines. As explained in the text, both types of contributions are suppressed compared to diagrams from Fig. 1 and will be disregarded in what follows.

whereas for the type- B contribution it is given by

$$\sum_{\ell n} \sigma_{\ell} \sigma_n c_{\ell n} \gamma(\mathbf{b}_{\ell}) \gamma(\mathbf{b}_n) = \frac{1}{4} [N(x, \mathbf{r}_{23}, \mathbf{b}_{23}) - N(x, \mathbf{r}_{24}, \mathbf{b}_{24}) + N(x, \mathbf{r}_{3,234}, \mathbf{b}_{2334}) - N(x, \mathbf{r}_{4,234}, \mathbf{b}_{2344}) + 2N(x, \mathbf{r}_{14}, \mathbf{b}_{24}) - 2N(x, \mathbf{r}_{13}, \mathbf{b}_{13})]. \quad (26)$$

The variables \mathcal{Y}_{ij} in Eqs. (22) and (23) stand for the lab-frame rapidity of the quark-antiquark pair made of partons i, j . Explicitly, they are given by

$$\mathcal{Y}_{ij} = \ln \left(\frac{(\alpha_i + \alpha_j) q^+}{M_{\perp}} \right), \quad (27)$$

where α_i and α_j are light-cone fractions of the heavy quarks that form a given quarkonium.

The dipole amplitude, which appears in Eqs. (25) and (26), effectively takes into account a sum of different Pomeron ladders [57,60], and for this reason it corresponds to the exchange of vacuum quantum numbers in the t channel. This fact imposes certain constraints on possible quantum numbers of heavy quarkonia produced via the $\gamma + IP \rightarrow M_1 M_2$ subprocess. Since the C parity of a photon is negative, the neutral quarkonia M_1, M_2 must have opposite C parities. This explicitly excludes production of quarkonia with the same quantum numbers ($M_1 = M_2$). For the case when quarkonia are charged (e.g., $B_c^+ B_c^-$), this implies that they necessarily must be produced with an odd value of the mutual angular momentum L . Finally, we need to mention that at higher orders the interaction with the target should be supplemented by the exchange of C -odd three-gluon ladders (so-called odderons) in the t channel [95], potentially giving contributions of odderon exchange, as shown in the right panel of Fig. 2. Such interactions are suppressed at high energies, because the odderon has a smaller intercept than the Pomeron. Besides, formally such contributions are also suppressed by $\mathcal{O}(\alpha_s(m_Q))$.

Another possibility to produce a C -even pair of quarkonia is via the exchange of a (C -odd) photon, as shown in the right panel of Fig. 2. Formally, such contributions are suppressed by $\sim \alpha_{\text{em}}/\alpha_s^2(m_Q)$, which is a small parameter for charm and bottom quarks, yet could get enhanced in the infinitely heavy quark mass limit $m_Q \rightarrow \infty$ due to the suppression of $\alpha_s(m_Q)$ in the denominator. Besides, this contribution can be enhanced in the very forward kinematics by the photon propagator $\sim 1/t$, where $t \equiv (p_f - p_i)^2$ is very small.² According to phenomenological analyses [30–34], the cross sections of this mechanism is much smaller numerically than that of the mechanism suggested in this paper. For this reason, in what follows we will focus on the production of opposite-parity quarkonia, and will disregard the contributions of t -channel odderons and photons altogether.

²Numerical estimates show that the invariant momentum transfer t for photoproduction of a pair of quarkonia M_1, M_2 is restricted by

$$|t| \gtrsim |t_{\min}(W)| \approx \frac{m_N^2 M_{12}^2}{W^2} + \mathcal{O}\left(\frac{m_N^2}{s}, \frac{M_{12}^2}{s}\right),$$

where m_N is the mass of the nucleon, $W^2 \equiv s_{\gamma p} = (q + P)^2$, and $M_{12}^2 = (p_{M_1} + p_{M_2})^2$ is the invariant mass of the quarkonia pair (clearly, $M_{12} \geq M_1 + M_2$). Already for EIC energies $W \sim 100$ GeV, so we can see that it is possible to achieve the kinematics of very small t even for heavy quarkonia.

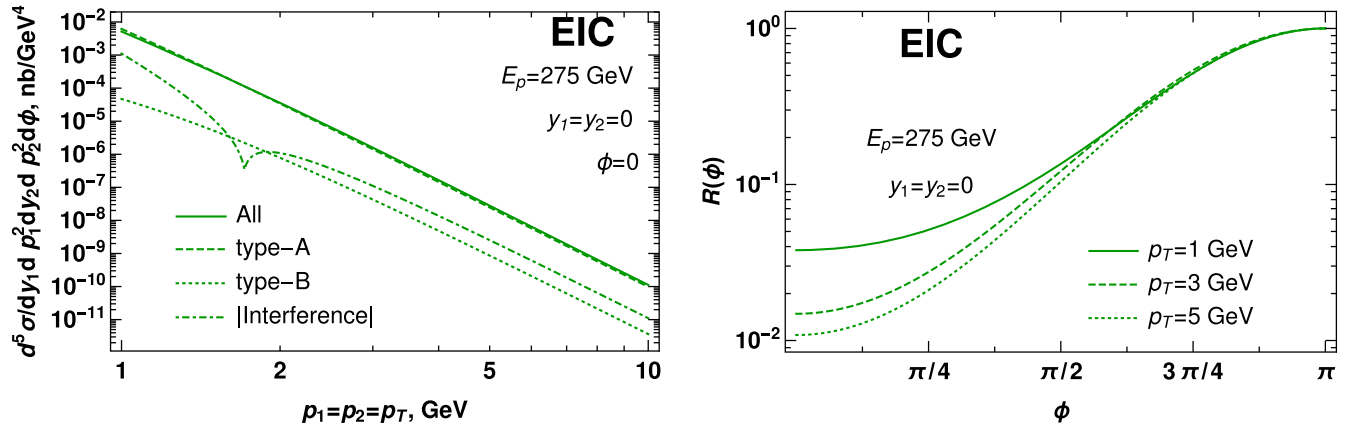


FIG. 3. Left: different contributions to charmonia pair photoproduction in EIC kinematics: type-A and type-B diagrams, as well as their interference. Right: dependence of the normalized ratio $R(\phi)$, defined in Eq. (36), on the angle ϕ (difference between azimuthal angles of both quarkonia). The appearance of a sharp peak in back-to-back kinematics is explained in the text. For definiteness we consider the case when both quarkonia are produced at central rapidities ($y_1 = y_2 = 0$) in the lab frame; for other rapidities, the ϕ dependence has a similar shape.

III. NUMERICAL RESULTS

The framework developed in the previous section is valid for heavy quarkonia of both c and b flavors. In what follows we will focus on the all-charm sector and present results for $J/\psi + \eta_c$ production, for which the cross section is larger and thus easier to study experimentally.³

For the wave function of the J/ψ mesons we will use a simple ansatz suggested in Refs. [96,97],

$$\begin{aligned} \Psi_{J/\psi}(z, \mathbf{r}, M=0) &= \frac{\delta_{h, -\bar{h}}}{\sqrt{2}} z(1-z)\varphi(z, \mathbf{r}), \\ \varphi(z, \mathbf{r}) &= \frac{\sqrt{2}\pi f_V}{\sqrt{N_c \hat{e}_V}} f(z) e^{-\omega^2 r^2/2}, \end{aligned} \quad (28)$$

$$\begin{aligned} \Psi_{J/\psi}(z, \mathbf{r}, M=\pm 1) &= \frac{1}{M_V} [iM e^{iM\theta} (\bar{z}\delta_{h, -M}\delta_{\bar{h}, M} - z\delta_{h, M}\delta_{\bar{h}, -M}) \partial_r \\ &+ m_Q \delta_{h, M}\delta_{\bar{h}, M}] \varphi(z, \mathbf{r}), \end{aligned} \quad (29)$$

$$f(z) = \sqrt{z(1-z)} e^{-M_V^2(z-1/2)^2/2\omega^2}, \quad (30)$$

where M is the helicity of J/ψ , \mathbf{r} is the distance between the quark and antiquark, h, \bar{h} are the helicities of the quark and antiquark, and f_V, e_V, ω are some numerical constants. This result can be trivially extended to the case of the η_c meson, which differs from the J/ψ meson only by the orientation of the quark spins. Taking into account the structure of the Clebsch-Gordan coefficients for the $1/2 \times 1/2$ product, we may immediately write out the

³According to our estimates, for bottomonia the cross sections are at least an order of magnitude smaller due to the heavier quark mass.

corresponding wave functions for η_c , modifying the corresponding $M=0$ component of the J/ψ wave function,

$$\Psi_{\eta_c}(z, \mathbf{r}) = \frac{\varepsilon_{h, \bar{h}}}{\sqrt{2}} z(1-z)\varphi(z, \mathbf{r}), \quad \varepsilon_{ab} = -\varepsilon_{ba} = \delta_{a, -b} \text{sign}(a). \quad (31)$$

Alternatively, the wave functions of quarkonia can be constructed using potential models or the well-known Brodsky-Huang-Lepage-Terentyev prescription [98–100], which allows to convert the rest-frame wave function Ψ_{RF} into a light-cone wave function Ψ_{LC} . It is known that in the small- r region, which is relevant for estimates, the wave functions of the S -wave heavy quarkonia in different schemes are quite close to each other [101–104], and for this reason in what follows we will use the ansatz of Eqs. (28)–(31), in view of its simplicity.

For our numerical evaluations we also need a parametrization of the dipole amplitude. In what follows we will use the impact parameter (b)-dependent “bCGC” parametrization of the dipole cross section [89,105],

$$N(x, \mathbf{r}, \mathbf{b}) = \begin{cases} N_0 \left(\frac{rQ_s(x)}{2}\right)^{2\gamma_{\text{eff}}(r)}, & r \leq \frac{2}{Q_s(x)}, \\ 1 - \exp(-\mathcal{A} \ln(BrQ_s)), & r > \frac{2}{Q_s(x)}, \end{cases} \quad (32)$$

$$\mathcal{A} = -\frac{N_0^2 \gamma_s^2}{(1-N_0)^2 \ln(1-N_0)}, \quad \mathcal{B} = \frac{1}{2}(1-N_0)^{\frac{1-N_0}{N_0 \gamma_s}}, \quad (33)$$

$$Q_s(x, \mathbf{b}) = \left(\frac{x_0}{x}\right)^{\lambda/2} T_G(b), \quad \gamma_{\text{eff}}(r) = \gamma_s + \frac{1}{\kappa \lambda Y} \ln\left(\frac{2}{rQ_s(x)}\right), \quad (34)$$

$$\gamma_s = 0.66, \quad \lambda = 0.206, \quad x_0 = 1.05 \times 10^{-3},$$

$$T_G(b) = \exp\left(-\frac{b^2}{2\gamma_s B_{\text{CGC}}}\right). \quad (35)$$

Since the dipole approach as a whole and the particular CGC parametrization (32) are applicable in the kinematics of small $x \lesssim 10^{-2} \ll 1$, in what follows we will consider only the kinematics of the highest energy runs at EIC, with $\sqrt{s_{\text{ep}}} \approx 141$ GeV. For smaller energies the contribution of Pomeron-mediated exchanges is suppressed, and sizable corrections from other mechanisms might become important.

We would like to start the presentation of numerical results with a discussion of the relative contribution of type-A and type-B diagrams introduced in the previous section. From the left panel of Fig. 3 we can see that the dominant contribution comes from the type-A diagrams. This enhancement can be partially explained by larger color factors in the large- N_c limit. The interference of type-A and type-B contributions represents approximately a 10% correction and moreover has a node, whose position depends on the produced quarkonia kinematics. As expected, the cross section is suppressed as a function of p_T (we consider $|\mathbf{p}_{J/\psi}^\perp| = |\mathbf{p}_{\eta_c}^\perp| = p_T$ for the sake of definiteness). In the right panel of the Fig. 3 we present the dependence of the yields on the azimuthal angle ϕ between the transverse momenta of the J/ψ and η_c mesons. For definiteness, we assumed that the transverse momenta $\mathbf{p}_{J/\psi}^\perp, \mathbf{p}_{\eta_c}^\perp$ of both quarkonia have equal absolute values. In order to make a meaningful comparison of the cross sections, which differ by orders of magnitude, we plot the normalized ratio

$$R(\phi) = \frac{d\sigma(\dots, \phi)/dy_1 dp_1^2 dy_2 dp_2^2 d\phi}{d\sigma(\dots, \phi = \pi)/dy_1 dp_1^2 dy_2 dp_2^2 d\phi}, \quad (36)$$

$$R(\phi = \pi) \equiv 1.$$

We can see that the ratio has a sharp peak in the back-to-back region ($\phi = \pi$), which happens because in this kinematics the momentum transfer to the target $|t| = |\Delta^2|$ is minimal. In contrast, for the angle $\phi \approx 0$, which maximizes the variable $|t| = |\Delta^2|$, the ratio has a pronounced dip. For $p_1 \neq p_2$ the dependence on ϕ is qualitatively similar, although the maximum and minimum are less pronounced.

In the left panel of Fig. 4 we analyze the p_T dependence, for the case when one of the quarkonia has a small transverse momentum $p_i \sim 1$ GeV. As expected, in this case the cross section has a significantly milder suppression compared to the case when both quarkonia share the same transverse momentum. This result indicates that the quarkonia pair are predominantly produced with small transverse momenta $p_1^\perp \sim p_2^\perp \lesssim 1$ GeV and opposite directions in the transverse plane ($\phi \equiv \phi_1 - \phi_2 \approx \pi$). In the right panel of Fig. 4 we show the p_T dependence of the cross section in LHeC kinematics. While the absolute value increases in this case, we may observe that qualitatively the dependence on p_T and the angle ϕ remains the same.

In Fig. 5 we analyze the dependence of the cross section on rapidities of the quarkonia. In the left panel we consider the special case when both quarkonia are produced with the same transverse momenta $p_1^\perp \sim p_2^\perp \sim 1$ GeV and the same rapidities $y_1 = y_2$ in the lab frame. The variables $y_{1,2}$ in this case can be unambiguously related to the invariant

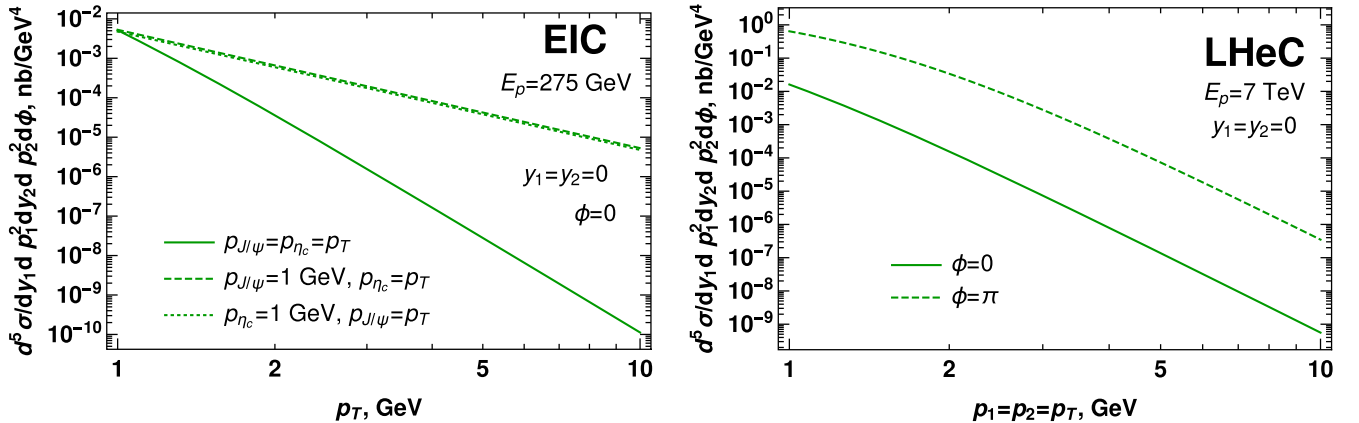


FIG. 4. Left: p_T dependence of the charmonia pair photoproduction cross section. Comparison of the p_T -dependence of the cross sections in different kinematics: (a) both quarkonia are produced with large transverse momentum (solid line) (b) one of the quarkonia has small momentum (dashed and dot-dashed lines). Within errors of numerical evaluation, there is no difference if the soft transverse momentum $p_T \approx 1$ GeV is assigned to J/ψ or η_c mesons. Right: p_T dependence of the cross section in LHeC kinematics. For definiteness we consider the case when both quarkonia are produced at central rapidities ($y_1 = y_2 = 0$) in the lab frame.

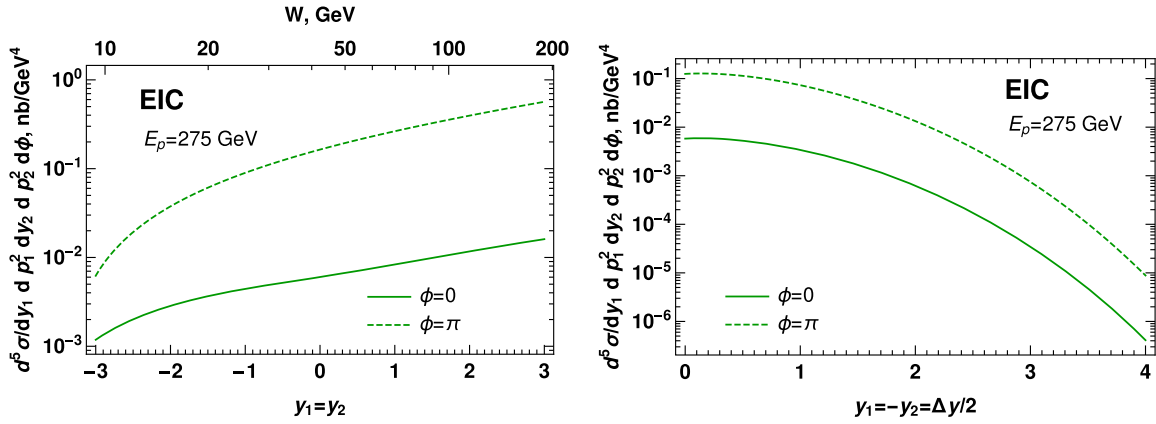


FIG. 5. Left: rapidity dependence of the photoproduction cross section in EIC kinematics, assuming equal rapidities of the produced quarkonia, $y_1 = y_2$. The upper horizontal scale illustrates the corresponding value of the invariant energy $W \equiv \sqrt{s_{\gamma p}}$ defined in Eq. (14). Right: dependence on the rapidity difference between the produced quarkonia, $y_1 = -y_2 = \Delta y/2$. For the sake of definiteness we assume that both quarkonia are produced at central rapidities ($y_1 = y_2 = 0$) with transverse momenta $p_1 = p_2 = 1$ GeV in the lab frame.

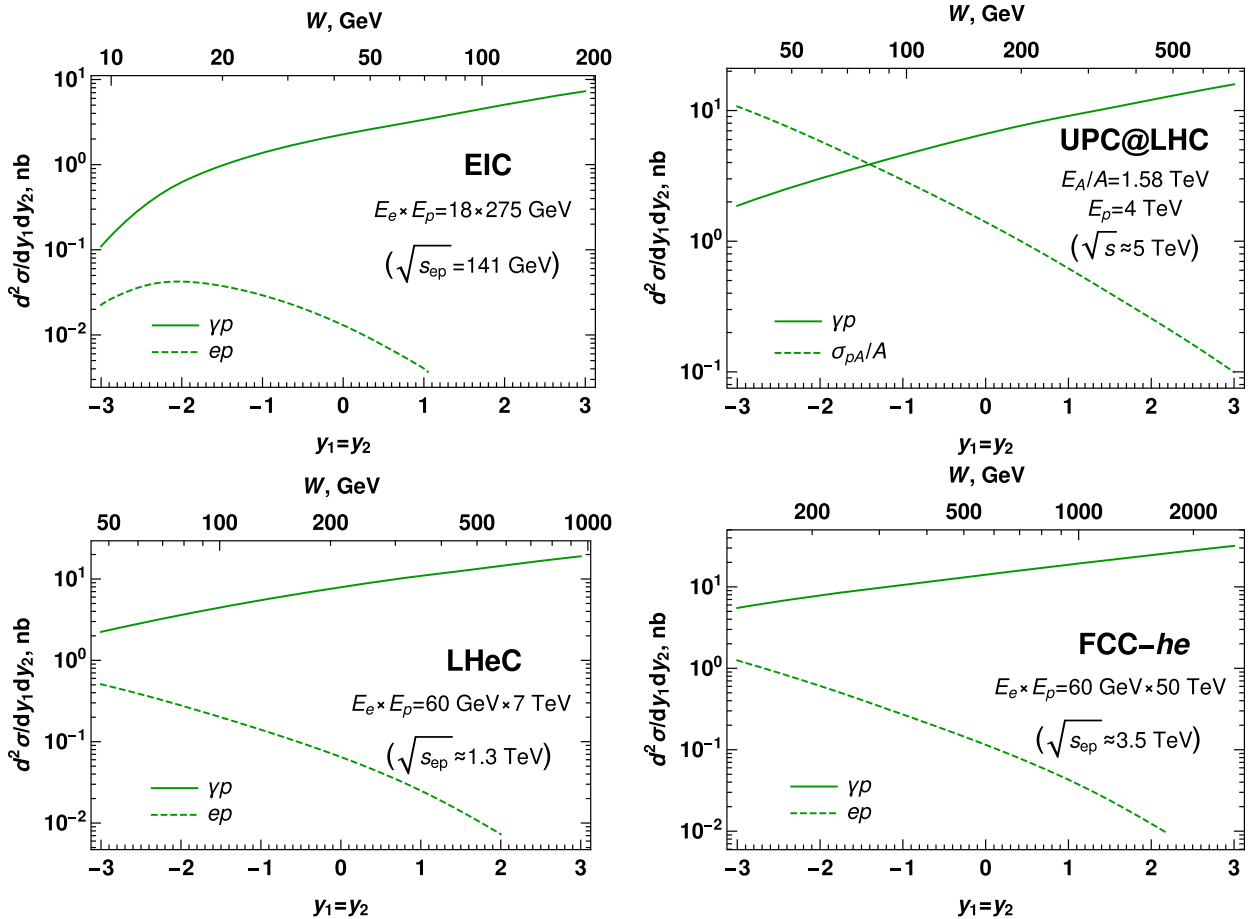


FIG. 6. Rapidity dependence of the p_T -integrated cross section in the kinematics of ultraperipheral collisions at the LHC and in the kinematics of the future ep colliders. A positive sign of rapidity is chosen in the direction of the electron or emitted quasireal photon. For ultraperipheral collisions the positive direction of rapidity is that of a heavy lead ion, and the cross sections are given per nucleon. The solid curves correspond to the cross section of the $\gamma p \rightarrow M_1 M_2 p$ subprocess, whereas dotted lines correspond to the cross sections of the complete physically observable ep or $A p$ processes. We assume for definiteness that the rapidities of both quarkonia are equal to each other in the lab frame, $y_1 = y_2 = y$. The upper horizontal scale illustrates the corresponding value of the invariant energy $W \equiv \sqrt{s_{\gamma p}}$, as defined in Eq. (14).

photon-proton energy $W_{\gamma p} \sim \sqrt{s_{\gamma p}}$ (shown on the upper horizontal axis) and, as expected, the cross section grows as a function of energy. In the right panel of Fig. 5 we analyze the dependence of the cross section on the rapidity difference Δy between two heavy mesons. For the sake of definiteness we consider that both quarkonia have opposite rapidities in the lab frame, $y_1 = -y_2 = \Delta y/2$. We observe that in this case the cross section becomes suppressed as a function of Δy , which illustrates the fact that the quarkonia are predominantly produced with the same rapidities.

Finally, in Figs. 6–8 we show the results for the cross section $d\sigma_{\gamma p \rightarrow M_1 M_2 p}/dy_1 dy_2$, which is integrated over the transverse momenta p_i^\perp of both quarkonia. This observable can be the most promising for experimental studies, since it is easier to measure. We make the predictions in the kinematics of the ultraperipheral pA collisions at LHC,

as well as future electron-hadron colliders. The dependence on y_1, y_2 largely repeats similar dependence of the p_T -unintegrated cross sections. This happens because the p_T -integrated cross sections get its dominant contributions from the region of small $p_T \ll m_Q$, where dependence on rapidity is mild. In Figs. 6 and 7 we also show the cross sections of the “master” processes $ep \rightarrow eM_1 M_2 p$ and $Ap \rightarrow AM_1 M_2 p$. The expressions for these cross sections differ from those of $\gamma p \rightarrow M_1 M_2 p$ by a convolution with known kinematic factors, which correspond to fluxes of equivalent photons generated by the electron or heavy nucleus. These cross sections have completely different dependence on the rapidity $y_1 = y_2$ of both quarkonia, which can be understood from Eqs. (8)–(16). Indeed, mesons with higher lab-frame rapidities can be produced by photons of higher energy E_γ , yet the flux of equivalent

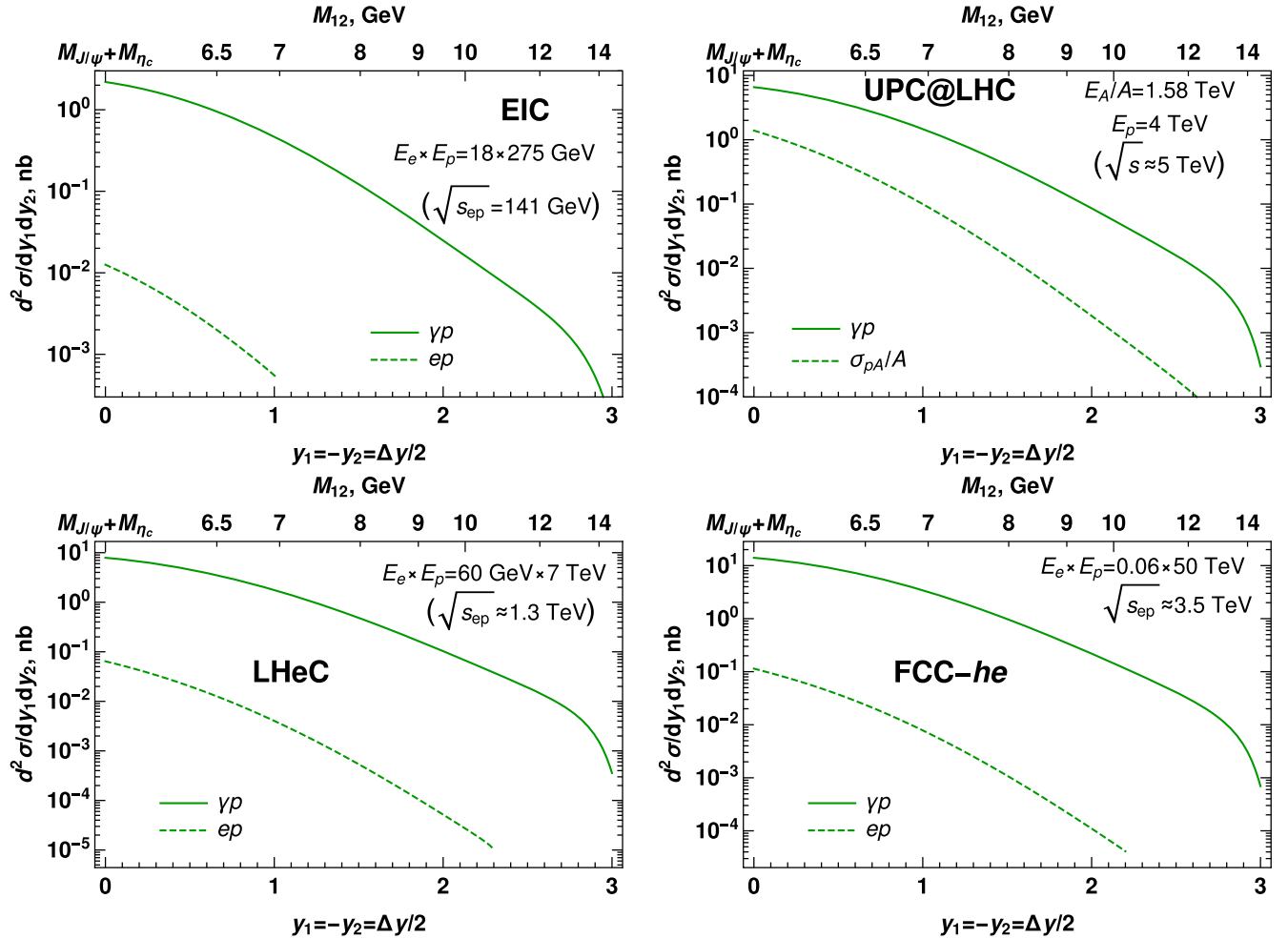


FIG. 7. Dependence on rapidity difference for the p_T -integrated cross section, in the kinematics of ultraperipheral collisions, at the LHC and future electron-proton colliders. The positive sign of rapidity is chosen in the direction of the electron or emitted quasireal photon. For ultraperipheral collisions the positive direction of rapidity is that of a heavy lead ion, and the cross sections are given per nucleon. For the sake of definiteness we assume that in the lab frame the quarkonia have opposite rapidities, $y_1 = -y_2 = \Delta y/2$. The upper horizontal scale illustrates the corresponding value of the invariant mass $M_{12} \equiv \sqrt{(p_{J/\psi} + p_{\eta_c})^2}$, as defined in Eq. (15). Dotted curves correspond to the cross sections of the complete process (electron-proton or heavy ion-proton).

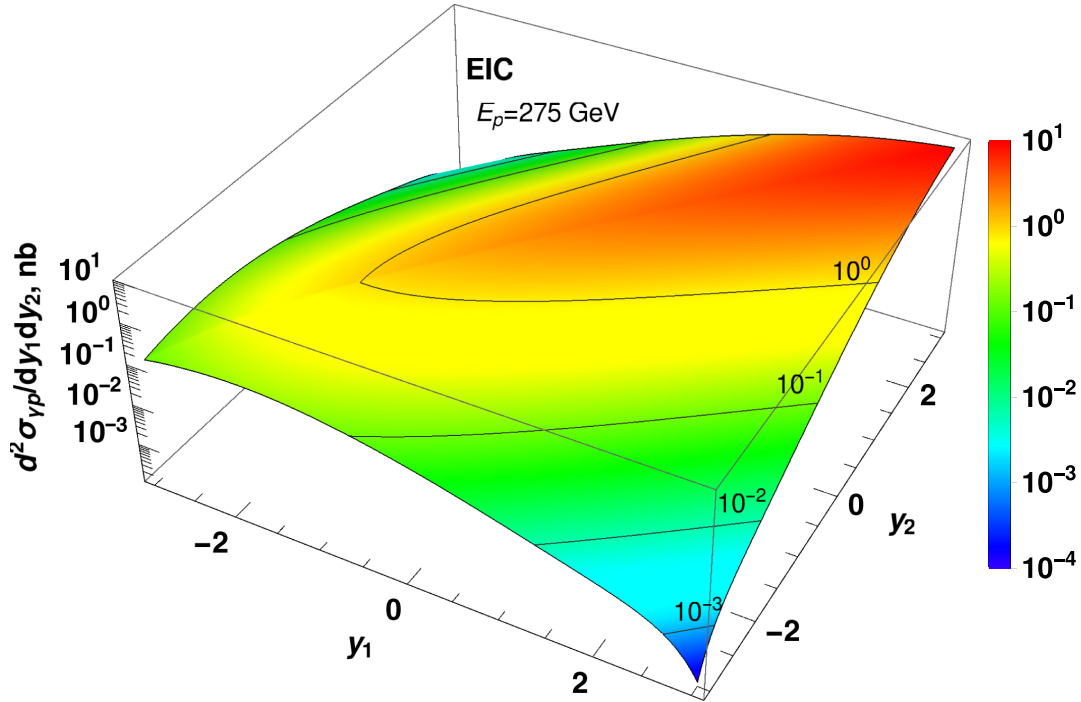


FIG. 8. Dependence on rapidities y_1, y_2 of produced quarkonia for the p_T -integrated photoproduction cross section $d\sigma_{\gamma p}/dy_1 dy_2$. The plot illustrates the fact that partons are produced with approximately equal rapidities, $y_1 \approx y_2$. For definiteness we consider a proton with the typical energy of EIC kinematics ($E_p \sim 275$ GeV in the lab frame). For other proton energies the dependence has a qualitatively similar shape.

photons created by a charged electron or ion is suppressed and vanishes when the elasticity $y = E_\gamma/E_e$ approaches unity. Finally, Fig. 8 illustrates how the cross section behaves as a function of y_1, y_2 in general, when $|y_1| \neq |y_2|$. We can see that the cross section has a typical ridge near $y_1 \approx y_2$, i.e., when quarkonia are produced with approximately the same rapidities.

IV. CONCLUSIONS

In this paper we studied in detail the exclusive photoproduction of heavy charmonia pairs. This process presents a lot of interest, both on its own as a potential test of quarkonia-production mechanisms in small- x kinematics, and as a background to exotic hadron production. We analyzed in detail the leading-order contributions and found that in this mechanism the quarkonia pairs are produced with opposite C parities, relatively small opposite transverse momenta p_T , and small separation in rapidity. This finding is explained by the fact that in the chosen kinematical region the momentum transfer to the recoil proton is minimal. As expected, the cross section decreases rapidly as a function of p_T , and grows as a function of the photon-proton invariant energy (\sim quarkonia rapidities), similar to single-photon production. However, the cross section decreases as a function of the rapidity difference between the quarkonia. We numerically estimated the cross section in the kinematics of ultraperipheral pA collisions at

the LHC, as well as in the kinematics of the future electron-proton colliders, and found that the cross section is sufficiently large for experimental studies. Our evaluation is largely parameter free and relies only on the choice of the parametrization for the dipole cross section (32) and wave functions of quarkonia.

We need to mention that earlier studies [30–35] of exclusive production focused on the production of quarkonia pairs with the same quantum numbers (e.g., $J/\psi J/\psi$), which means that this process predominantly proceeds via the exchange of *two* photons at the amplitude level, like, e.g., via photon-photon fusion $\gamma\gamma \rightarrow M_1 M_2$ [30–34] or double-photon scattering [35]. Due to the extra virtual photon in the amplitude, the cross sections of such processes are parametrically suppressed by $\sim \alpha_{\text{em}}^2$ compared to the cross section of opposite- C -parity quarkonia, and thus numerically are significantly smaller. Most studies [30–35] presented their predictions for the cross section of the $\gamma\gamma \rightarrow J/\psi J/\psi$ subprocess, which precludes a direct comparison with our results in view of the different underlying mechanism. A meaningful comparison can be done for the cross sections of the full exclusive process $pp \rightarrow pp M_1 M_2$ in ultraperipheral kinematics, which has been analyzed in Ref. [31]. In Fig. 9 we directly compare the results presented in Ref. [31] with the cross section evaluated in the framework of Sec. II. As expected, the cross section of our mechanism is larger than for the $\gamma\gamma$ -fusion-mediated production, though the enhancement is slightly milder than the naively expected $\sim 1/\alpha_{\text{em}}^2$.

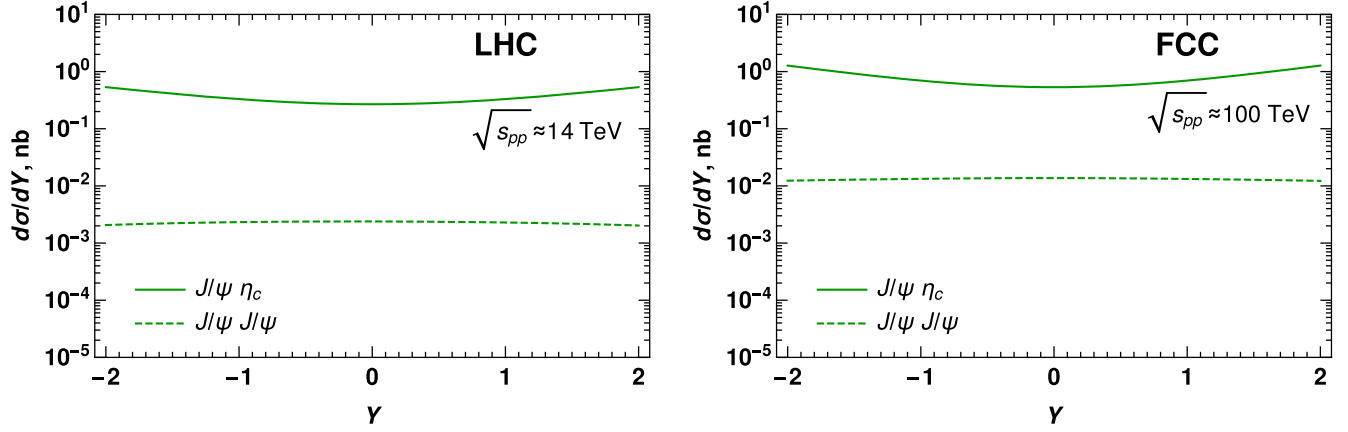


FIG. 9. Cross sections of different quarkonia-production mechanisms in the exclusive $pp \rightarrow ppM_1M_2$ process. The mechanism of this paper leads to the production of quarkonia with opposite C parity ($J/\psi\eta_c$ pairs). The theoretical expectations for $J/\psi J/\psi$ production (via photon-photon fusion) are taken from Ref. [31]. The left and right plots differ only by the value of the collision energy $\sqrt{s_{pp}}$. Following Ref. [31], we consider that both quarkonia are produced with the same rapidity $Y = y_1 = y_2$ in the lab frame; the cross section is integrated over all other kinematical variables.

We hope that the process suggested in this paper will be included in the program of the future EIC collider, as well as ongoing studies at the LHC in ultraperipheral kinematics. Finally, we need to mention that it is quite straightforward to extend the framework developed in this manuscript to the case of all-heavy tetraquark production; for this, it is only necessary that the product of the final-state quarkonia wave functions in Eqs. (22) and (23) be replaced with the wave function of the tetraquark state. Estimates of the cross sections for this case will be presented in a separate publication.

ACKNOWLEDGMENTS

We thank our colleagues at Universidad Técnica Federico Santa María for encouraging discussions. This research was partially supported by projects Proyecto ANID PIA/APOYO AFB180002 (Chile) and Fondecyt Regular (Chile) Grants No. 1180232 and No. 1220242. The research of S. A. was partially supported by the Fellowship Program ANID BECAS/MAGÍSTER NACIONAL (Chile) No. 22200123. Powered@NLHPC: This research was partially supported by the supercomputing infrastructure of the NLHPC (ECM-02).

APPENDIX A: HIGH-ENERGY SCATTERING IN THE COLOR DIPOLE PICTURE

In this Appendix, for the sake of completeness we briefly recall the general procedure that allows to express different hard amplitudes in terms of the *color-singlet* forward dipole scattering amplitude. While in the literature there are several equivalent formulations [47,49–55], in what follows we will use the Iancu-Mueller approach [106].

The natural hard scale, which controls the interaction of a heavy quark with the gluonic field, is its mass m_Q . In the

heavy quark mass limit we may formally develop a systematic expansion over $\alpha_s(m_Q) \ll 1$. Furthermore, for small color-singlet dipoles there is an additional suppression by the dipole size, $r \sim 1/m_Q$, so the interaction of singlet dipoles with perturbative gluons is suppressed at least as $\sim \alpha_s(m_Q)/m_Q$. However, the interaction of gluons with each other, as well as with light quarks, remains strongly nonperturbative in the deeply saturated regime, so we expect that the dynamics of the dipole amplitudes should satisfy the nonlinear Balitsky-Kovchegov equation.

At very high energies the dynamics of partons can be described in the eikonal approximation. The transverse coordinates of the high-energy partons remain essentially frozen during their propagation in the gluonic field dipole of the target. Similarly, due to eikonal interactions we may completely disregard the change of the quark helicities. In this picture the interaction of a dipole with the target is described by the S -matrix element [60,106]

$$S(y, \mathbf{x}_Q, \mathbf{x}_{\bar{Q}}) = \frac{1}{N_c} \langle \text{tr}(V^\dagger(\mathbf{x}_Q)V(\mathbf{x}_{\bar{Q}})) \rangle, \quad (\text{A1})$$

where we use the notation $y = \ln(1/x)$ for the dipole rapidity, $\mathbf{x}_Q, \mathbf{x}_{\bar{Q}}$, are the transverse coordinates of the partons (quark or antiquark), and the factors $V^\dagger(\mathbf{x}_Q)$ and $V(\mathbf{x}_{\bar{Q}})$ in Eq. (A1) are the Wilson lines, which describe the interaction of the partons with the color field of a hadron. They can be expressed as

$$V(\mathbf{x}_\perp) = P \exp\left(ig \int dx^- A_a^+(x^-, \mathbf{x}_\perp) t^a\right), \quad (\text{A2})$$

where A_μ^a is the gluonic field in a hadron. The impact-parameter-dependent dipole amplitude $N(x, \mathbf{r}, \mathbf{b})$ can be related to $S(y, \mathbf{x}_Q, \mathbf{x}_{\bar{Q}})$ as

$$N(x, \mathbf{r}, \mathbf{b}) = 1 - S(y, \mathbf{x}_Q, \mathbf{x}_{\bar{Q}}), \quad (\text{A3})$$

where the variable $\mathbf{r} \equiv \mathbf{x}_Q - \mathbf{x}_{\bar{Q}}$ is the transverse size of the dipole, $\mathbf{b} \equiv z\mathbf{x}_Q + (1-z)\mathbf{x}_{\bar{Q}}$ is the transverse position of the dipole center of mass, and z is the fraction of the light-cone momentum of a dipole which is carried by the quark Q . In view of the weakness of the interaction between heavy quarks and gluons, we can make an expansion of the exponent in Eq. (A2) over $\alpha_s(m_Q)$. In this approximation the effective interaction of the quark or antiquark with the gluonic field of the proton can be described by the factor $\pm i t^a \gamma_a(\mathbf{x}_\perp)$, where \mathbf{x}_\perp is the transverse coordinate of the quark,

$$\gamma_a(\mathbf{x}) = g \int dx^- A_a^+(x^-, \mathbf{x}), \quad (\text{A4})$$

and t_a are the ordinary color group generators of perturbative quantum chromodynamics in the fundamental representation. Inspired by the color structure of the interaction, in what follows we will refer to these interactions as ‘‘exchanges of t -channel Pomeron (gluons),’’ tacitly assuming that it can include cascades (showers) of particles. For the dipole scattering amplitude (A3), using Eqs. (A1) and (A4), we obtain

$$N(x, \mathbf{r}, \mathbf{b}) \approx \frac{1}{2} [\gamma_a(\mathbf{x}_Q) - \gamma_a(\mathbf{x}_{\bar{Q}})]^2. \quad (\text{A5})$$

For further evaluations it is more convenient to rewrite this result in the form

$$\gamma_a(\mathbf{x}_1)\gamma_a(\mathbf{x}_2) = -N(x, \mathbf{r}_{12}, \mathbf{b}_{12}) + \frac{\rho(\mathbf{x}_1) + \rho(\mathbf{x}_2)}{2}, \quad (\text{A6})$$

where we defined the shorthand notation $\rho(\mathbf{x}_a) \equiv |\gamma_a(\mathbf{x})|^2$, and $\mathbf{r}_{12}, \mathbf{b}_{12}$ are the distance and center of mass of the quark-antiquark pair located at points $\mathbf{x}_1, \mathbf{x}_2$. For many processes the contributions $\sim \rho(\mathbf{x}_i)$ cancel, so the amplitude can eventually be represented as a linear superposition of the dipole amplitudes $N(x, \mathbf{r}, \mathbf{b})$. In what follows, we will see that the amplitude of the process considered in this manuscript can be represented as a bilinear combination of terms with structure $\sim [\gamma(\mathbf{x}_i) - \gamma(\mathbf{x}_j)]$. For this special case the substitution of Eq. (A6) allows to get a few important identities between bilinear expressions:

$$\begin{aligned} & [\gamma_a(\mathbf{x}_1) - \gamma(\mathbf{x}_2)][\gamma_a(\mathbf{x}_3) - \gamma_a(\mathbf{x}_4)] \\ &= N(x, \mathbf{r}_{23}, \mathbf{b}_{23}) + N(x, \mathbf{r}_{14}, \mathbf{b}_{14}) - N(x, \mathbf{r}_{13}, \mathbf{b}_{13}) \\ & \quad - N(x, \mathbf{r}_{24}, \mathbf{b}_{24}), \end{aligned} \quad (\text{A7})$$

$$\begin{aligned} & [\gamma_a(\mathbf{x}_1) - \gamma_a(\mathbf{x}_2)][\gamma_a(\mathbf{x}_3) + \gamma_a(\mathbf{x}_4) - 2\gamma_a(\mathbf{x}_5)] \\ &= N(x, \mathbf{r}_{23}, \mathbf{b}_{23}) + N(x, \mathbf{r}_{24}, \mathbf{b}_{24}) - N(x, \mathbf{r}_{13}, \mathbf{b}_{13}) \\ & \quad - N(x, \mathbf{r}_{14}, \mathbf{b}_{14}) + 2[N(x, \mathbf{r}_{15}, \mathbf{b}_{15}) - N(x, \mathbf{r}_{25}, \mathbf{b}_{25})], \end{aligned} \quad (\text{A8})$$

$$\begin{aligned} & [\gamma_a(\mathbf{x}_1) + \gamma_a(\mathbf{x}_2) - 2\gamma_a(\mathbf{x}_3)]^2 \\ &= 2N(x, \mathbf{r}_{13}, \mathbf{b}_{13}) + 2N(x, \mathbf{r}_{23}, \mathbf{b}_{23}) - N(x, \mathbf{r}_{12}, \mathbf{b}_{12}), \end{aligned} \quad (\text{A9})$$

where \mathbf{r}_{ij} and \mathbf{b}_{ij} are the relative distance and center of mass of the quark-antiquark pair located at points $\mathbf{x}_i, \mathbf{x}_j$.

For the impact-parameter-independent (\mathbf{b} -integrated) cross section, the results (A5)–(A7) can be rewritten in a simpler form:

$$\begin{aligned} N(x, \mathbf{r}) &= \frac{1}{2} \int d^2b |\gamma_a(x, \mathbf{b} - z\mathbf{r}) - \gamma_a(x, \mathbf{b} + \bar{z}\mathbf{r})|^2, \quad (\text{A10}) \\ \int d^2b \gamma_a(x, \mathbf{b}) \gamma_a(x, \mathbf{b} + \mathbf{r}) &= -N(x, \mathbf{r}) + \underbrace{\int d^2b |\gamma_a(x, \mathbf{b})|^2}_{=\text{const}}. \end{aligned} \quad (\text{A11})$$

The value of the constant term on the right-hand side of Eq. (A11) is related to the infrared behavior of the theory, and for the observables which we consider in this paper, it cancels exactly. In what follows we will apply this formalism to the evaluation of the exclusive di-meson production amplitudes.

APPENDIX B: EVALUATION OF THE PHOTON WAVE FUNCTION

For evaluation of the photon wave function we follow the standard rules of the light-cone perturbation theory formulated in Refs. [16,107]. The result for the $\bar{Q}Q$ component is well known in the literature [96,108], yet in Appendix B 1 we will briefly repeat its derivation in order to introduce notations. As we will see later in Appendix B 2, the wave function of the $\bar{Q}Q\bar{Q}Q$ component can be expressed in terms of the wave function of the $\bar{Q}Q$ component. In our evaluation we will focus on on-shell transversely polarized photons, which give the dominant contribution, unless some specific cuts are imposed on its virtuality Q^2 . The momentum of the photon (1) introduced earlier simplifies in this case and has only a light-cone component in the plus-axis direction,

$$q \approx (q^+, 0, \mathbf{0}_\perp). \quad (\text{B1})$$

The polarization vector of the transversely polarized photon is given by

$$\epsilon_T^\mu(q) \equiv \left(0, \frac{\mathbf{q}_\perp \cdot \boldsymbol{\epsilon}_\gamma}{q^+}, \boldsymbol{\epsilon}_\gamma \right) \approx (0, 0, \boldsymbol{\epsilon}_\gamma), \quad (\text{B2})$$

$$\boldsymbol{\epsilon}_\gamma = \frac{1}{\sqrt{2}} \begin{pmatrix} 1 \\ \pm i \end{pmatrix}, \quad \gamma = \pm 1, \quad (\text{B3})$$

where in Eq. (B2) we took into account that $\mathbf{q}_\perp = 0$.

Before the interaction with the target, the photon might fluctuate into virtual quark-antiquark pairs, as well as gluons. In what follows we will use the convenient shorthand notation $\alpha_i = k_i/q^+$ for the fraction of light-cone momentum of the photon carried by each parton, as well as $\mathbf{k}_{i\perp}$ for the transverse component of the parton's momentum. In view of 4-momentum conservation we expect that $\alpha_i, \mathbf{k}_{i\perp}$ should satisfy the identity

$$\sum_i \alpha_i = 1, \quad \sum_i \mathbf{k}_{i\perp} = 0, \quad (\text{B4})$$

where summation is done over all partons. We may observe that the vector $\boldsymbol{\varepsilon}_\gamma$ satisfies the identity

$$\boldsymbol{\varepsilon}_\gamma^* \equiv \boldsymbol{\varepsilon}_{-\gamma}, \quad (\text{B5})$$

and its scalar product with any 2-vector a yields

$$\boldsymbol{\varepsilon}_\gamma \cdot \mathbf{a} = \frac{a_x + i\gamma a_y}{\sqrt{2}} = \frac{|a|}{\sqrt{2}} e^{i\gamma \arg(a)}, \quad \arg(a) = \arctan\left(\frac{a_y}{a_x}\right). \quad (\text{B6})$$

1. $\bar{Q}Q$ component of the photon wave function

In this section, for the sake of completeness we would like to recall the main steps in the derivation of the $\bar{Q}Q$ -component photon wave function [96,108] in the mixed (α, \mathbf{r}) representation. At leading order, the subprocess $\gamma \rightarrow \bar{Q}Q$ gets contributions only from the diagram shown in the left panel of Fig. 10. A bit later we will see that $\gamma \rightarrow \bar{Q}Q$, as well as the closely related $g \rightarrow \bar{Q}Q$ subprocess, appear as constituent blocks in the more complicated four-quark wave function. For this reason, in order to facilitate further discussion, in this section we will temporarily assume that the photon momentum q might have a nonzero transverse part \mathbf{q}_\perp , and use the notation $z = k_1^+/q^+$ for the fraction of light-cone momentum carried by the quark. In momentum space the evaluation is straightforward, using the rules from Refs. [16,107,109], and yields

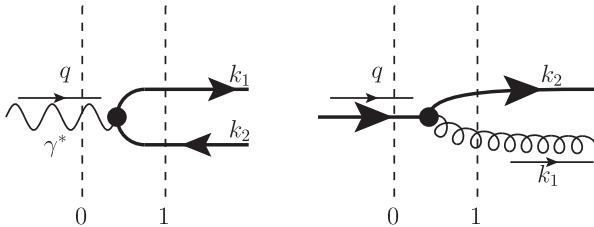


FIG. 10. Left: leading-order contributions to the $\bar{Q}Q$ component of the photon wave function $\psi_{g \rightarrow \bar{Q}Q}$. Right: so-called gluon emission wave function, as defined in Ref. [109]. The momenta k_i shown on the right-hand side are Fourier conjugates of the coordinates x_i .

$$\psi_{h\bar{h}}^\lambda(z, k_1, \mathbf{q}) = -e_q \delta_{c\bar{c}} \frac{\bar{u}_h(k_1) \hat{\varepsilon}_\lambda(q) v_{\bar{h}}(q - k_1)}{\Delta_{01}^- \sqrt{k_1^+} \sqrt{q^+ - k_1^+}}, \quad (\text{B7})$$

$$\Delta_{01}^- = -\frac{1}{2p^+} \frac{\mathbf{n}^2 + m_q^2}{z(1-z)}, \quad (\text{B8})$$

where λ is the helicity of the incoming photon, h, \bar{h} are the helicities of the produced quark and antiquark, c, \bar{c} are the color indices of Q and \bar{Q} , respectively, and e_q is the electric charge corresponding to a given heavy flavor. The momentum \mathbf{n} is defined as $\mathbf{n} = \mathbf{k}_1 - z\mathbf{q}_\perp = (1-z)\mathbf{k}_1 - z\mathbf{k}_2$ and physically has the meaning of the transverse part of the relative (internal) momentum of the $Q\bar{Q}$ pair. The numerator of Eq. (B7) can be written out explicitly using the rules from Refs. [96,108],

$$\begin{aligned} & \bar{u}_h(k) \hat{\varepsilon}_\lambda(p) v_{\bar{h}}(p - k) \\ &= \frac{2}{\sqrt{z(1-z)}} \left[(z\delta_{\lambda,h} - (1-z)\delta_{\lambda,-h}) \delta_{h,-\bar{h}} \mathbf{n} \cdot \boldsymbol{\varepsilon}_\lambda \right. \\ & \quad \left. + \frac{1}{\sqrt{2}} m_q \text{sign}(h) \delta_{\lambda,h} \delta_{h,\bar{h}} \right]. \end{aligned} \quad (\text{B9})$$

In configuration space the corresponding wave function can be found by making a Fourier transformation over the transverse momenta,

$$\begin{aligned} & \int \frac{d^2 k_1}{(2\pi)^2} \frac{d^2 k_2}{(2\pi)^2} e^{i(k_1 r_1 + k_2 r_2)} (2\pi)^2 \delta(\mathbf{k}_1 + \mathbf{k}_2 - \mathbf{q}) \psi_{h\bar{h}}^\lambda(z, k_1, \mathbf{q}) \\ &= e^{iq \cdot (z\mathbf{r}_1 + \bar{z}\mathbf{r}_2)} e_q \delta_{c\bar{c}} \Psi_{h\bar{h}}^\lambda(z, \mathbf{r}_{12}, m_q, m_q), \end{aligned} \quad (\text{B10})$$

where the integral over k_2 was performed using the properties of the δ function, and before the integration over \mathbf{k}_1 we shifted the integration variable as $\mathbf{k}_1 \rightarrow \mathbf{n} + z\mathbf{q}$. Explicitly, the integration over the variable $d^2 \mathbf{n}$ yields

$$\begin{aligned} \Psi_{h\bar{h}}^\lambda(z, \mathbf{r}_{12}, m_q, a) &= -\frac{2}{(2\pi)} \left[(z\delta_{\lambda,h} - (1-z)\delta_{\lambda,-h}) \delta_{h,-\bar{h}} i\boldsymbol{\varepsilon}_\lambda \right. \\ & \quad \left. \cdot \nabla - \frac{m_q}{\sqrt{2}} \text{sign}(h) \delta_{\lambda,h} \delta_{h,\bar{h}} \right] K_0(a\mathbf{r}). \end{aligned} \quad (\text{B11})$$

The structure of Eq. (B10) clearly suggests that in a mixed representation the variable $z\mathbf{r}_1 + \bar{z}\mathbf{r}_2$ plays the role of the dipole center of mass, whereas \mathbf{r}_{12} is its separation, in agreement with earlier findings from Ref. [110]. For the incoming off-shell photon with virtuality $-q^2 = Q^2$, in a similar fashion straightforward integration yields

$$e^{iq \cdot (z\mathbf{r}_1 + \bar{z}\mathbf{r}_2)} e_q \delta_{c\bar{c}} \Psi_{h\bar{h}}^\lambda\left(z, \mathbf{r}_{12}, m_q, \sqrt{m_q^2 - Q^2 z(1-z)}\right) \quad (\text{B12})$$

in the second line of Eq. (B10). The extension of this result for the production of a $Q\bar{Q}$ pair by a gluon is

straightforward and requires the simple replacement $e_q \delta_{c\bar{c}} \rightarrow g(t_a)_{c\bar{c}}$.

Finally, we would like to briefly discuss the so-called parton-level wave function of the gluon emission subprocess $q \rightarrow gq$, as introduced in Ref. [109]. This object is useful for the analysis of different amplitudes, as we will see in the next section. At the leading order it gets contributions from the diagram shown in the right panel of Fig. 10. The evaluation of this object is quite similar to the derivation of Eqs. (B7)–(B11). In momentum space we obtain

$$\tilde{\psi}_{c_f h_f, c_i h_i}^\lambda(z, k_1, \mathbf{q}) = -gt_{c_f c_i}^a \frac{\bar{u}_{h_f}(q - k_1) \hat{\epsilon}_\lambda(k_1) u_{h_i}(q)}{\Delta_{02}^- \sqrt{q^+} \sqrt{q^+ - k_1^+}}, \quad (\text{B13})$$

$$\Delta_{02}^- = -\frac{1}{2p^+} \frac{\mathbf{n}^2 + z^2 m_q^2}{z(1-z)}, \quad \mathbf{n} = \mathbf{k}_1 - z\mathbf{q}, \quad (\text{B14})$$

where λ is the helicity of the outgoing gluon, (h_i, c_i) and (h_f, c_f) are the helicities and color indices of the incident and final quark (before and after emission of a gluon), and (similar to the previous case) we have introduced the momentum $\mathbf{n} = \mathbf{k}_1 - z\mathbf{q} = (1-z)\mathbf{k}_1 - z\mathbf{k}_2$ which corresponds to the relative motion of the quark and gluon after the emission of the latter. Using the rules from Refs. [96,108], we may rewrite the numerator as

$$\begin{aligned} & \bar{u}_{h_f}(q - k_1) \hat{\epsilon}_\lambda(k_1) u_{h_i}(q) \\ &= \frac{2}{z\sqrt{1-z}} \left[(\delta_{\lambda, h_i} + (1-z)\delta_{\lambda, -h_i}) \delta_{h_i, h_f} \mathbf{n} \cdot \boldsymbol{\epsilon}_\lambda \right. \\ & \quad \left. - \frac{m_q}{\sqrt{2}} z^2 \text{sign}(h_i) \delta_{\lambda, -h_i} \delta_{h_i, -h_f} \right]. \end{aligned}$$

In configuration space the corresponding wave function is given by

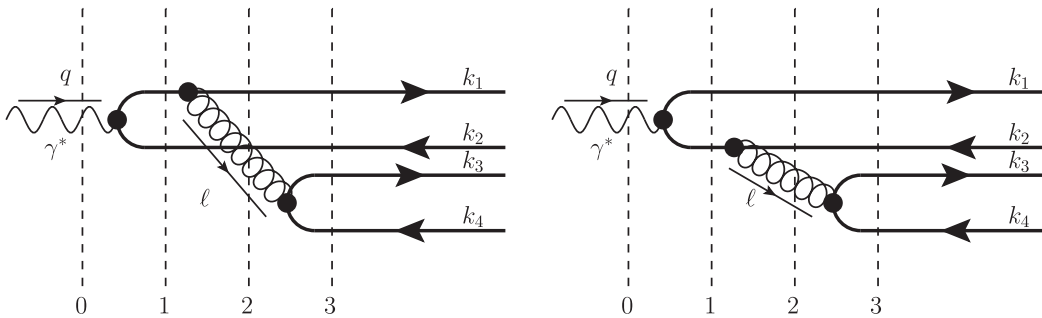


FIG. 11. Leading-order contribution to the wave function $\psi_{\bar{Q}Q\bar{Q}Q}^{(\gamma)}$ defined in the text. The momenta k_i shown on the right-hand side are Fourier conjugates of the coordinates x_i . It is implied that both diagrams should be supplemented by all possible permutations of final-state quarks (see the text for more details).

$$\begin{aligned} & \int \frac{d^2 k_1}{(2\pi)^2} \frac{d^2 k_2}{(2\pi)^2} e^{i(\mathbf{k}_1, \mathbf{r}_1 + \mathbf{k}_2, \mathbf{r}_2)} (2\pi)^2 \\ & \quad \times \delta(\mathbf{k}_1 + \mathbf{k}_2 - \mathbf{q}) \psi_{c_f h_f, c_i h_i}^\lambda(z, k_1, \mathbf{q}) \\ &= e^{i\mathbf{q} \cdot (z\mathbf{r}_1 + \bar{z}\mathbf{r}_2)} t_{c_f c_i}^a \Phi_{h_f, h_i}^\lambda(z, \mathbf{r}_{12}, m_q, z m_q), \quad (\text{B15}) \end{aligned}$$

where the integral over k_2 is performed using the properties of the wave function, and integration over the variable $\mathbf{k}_1 = \mathbf{n} + z\mathbf{q}$ yields

$$\begin{aligned} & \Phi_{h_f, h_i}^\lambda(z, \mathbf{r}_{12}, m_q, a) \\ &= -\frac{2}{(2\pi)} \left[(\delta_{\lambda, h_i} + (1-z)\delta_{\lambda, -h_i}) \delta_{h_i, h_f} i\boldsymbol{\epsilon}_\lambda \right. \\ & \quad \left. \cdot \nabla + \frac{m_q}{\sqrt{2}} z^2 \text{sign}(h_i) \delta_{\lambda, -h_i} \delta_{h_i, -h_f} \right] K_0(a\mathbf{r}). \quad (\text{B16}) \end{aligned}$$

For the case of an incoming off-shell quark with virtuality Q^2 , a straightforward generalization shows that the second line of Eq. (B15) takes the form

$$e^{i\mathbf{q} \cdot (z\mathbf{r}_1 + \bar{z}\mathbf{r}_2)} \Phi_{h_f, h_i}^\lambda(z, \mathbf{r}_{12}, m_q, \sqrt{m_q^2 z - Q^2 z(1-z)}). \quad (\text{B17})$$

Similar to the previous case, the structure of Eq. (B16) clearly suggests that in a mixed representation the variable $z\mathbf{r}_1 + \bar{z}\mathbf{r}_2$ plays the role of the dipole center of mass, whereas \mathbf{r}_{12} is its separation [110].

2. $\bar{Q}Q\bar{Q}Q$ component of the photon wave function

As mentioned earlier in Appendix A, in the eikonal approximation the amplitude of the subprocess $\gamma^* \rightarrow \bar{Q}Q\bar{Q}Q$ in configuration space can be represented as a convolution of the wave function $\psi_{\bar{Q}Q\bar{Q}Q}^{(\gamma)}$ with linear combinations of dipole amplitudes (A7). At leading order over α_s the amplitude of the process is given by the two diagrams shown in Fig. 11. It should be understood that these diagrams should be supplemented by all possible permutations of final-state quarks. More precisely, for the

production of different heavy flavors (e.g., $\bar{c}c\bar{b}b$) both diagrams should be supplemented by contributions with permuted *pairs* of momenta $(k_1, k_2) \leftrightarrow (k_3, k_4)$. For the same-flavor quarkonia pairs (e.g., $\bar{c}c\bar{c}c$) we should take into account contributions with independent permutations of the quarks and antiquarks: $k_1 \leftrightarrow k_3$ and $k_2 \leftrightarrow k_4$. The evaluation of the corresponding process follows the standard light-cone rules formulated in Refs. [16,107]. We need to mention that some blocks, which will be needed for the construction of the amplitude, have already been evaluated in Refs. [109,111] (although in the chiral limit only). In this section we extend those studies, and represent them in a form convenient for further analysis. According to the general light-cone rules [96,108], in the evaluation of the diagrams in Fig. 11 each propagator of the virtual (intermediate) parton has instantaneous and noninstantaneous parts. For technical reasons it is convenient to analyze the two types of contributions separately.

a. Noninstantaneous contributions

At leading order over α_s , the amplitude of the process is given by the two diagrams shown in Fig. 11 and depends on the momenta of the four quarks in the final state. In what follows we will use the standard notation $\alpha_i = k_i/q^+$ for the fractions of photon momentum carried by each of these fermions, as well as $\mathbf{k}_{i\perp}$ for the transverse components of their momenta. We also will use the shorthand notation $\ell = k_3 + k_4$ for the momentum of the virtual gluon connecting different quark lines. For the sake of generality, we will assume that the produced quark-antiquark pairs have different flavors, and will use the notations m_1 for the current mass of the quark line connected to a photon and m_2 for the current masses of the quark-antiquark pair produced from the virtual gluon.

Using the rules from Refs. [96,108], we may obtain for the corresponding amplitude of the subprocess

$$\begin{aligned} \mathcal{A}_{c_1 c_2, c_3 c_4}^{a_1 a_2, a_3 a_4} = & -\frac{e_q g^2 (t_a)_{c_1 c_2} \otimes (t_a)_{c_3 c_4}}{16\pi^2} \left(\frac{\bar{u}_{a_1}(k_1) \hat{\epsilon}_\lambda^*(\ell) u_b(k_1 + \ell) \bar{u}_b(q - k_2) \hat{\epsilon}_\gamma(q) v_{a_2}(k_2)}{D_{11} D_{12} D_{13} \sqrt{k_1^+} \sqrt{k_1^+ + \ell^+} \sqrt{q^+ - k_2^+} \sqrt{k_2^+}} \right. \\ & \left. + \frac{\bar{u}_{a_1}(k_1) \hat{\epsilon}_\gamma(q) v_b(q - k_1) \bar{v}_b(k_2 + \ell) \hat{\epsilon}_\lambda^*(\ell) v_{a_2}(k_2)}{D_{21} D_{22} D_{23} \sqrt{k_1^+} \sqrt{q^+ - k_1^+} \sqrt{k_2^+ + \ell^+} \sqrt{k_2^+}} \right) \frac{\bar{u}_{a_3}(k_3) \hat{\epsilon}_\lambda(\ell) v_{a_4}(k_4)}{(k_3^+ + k_4^+) \sqrt{k_3^+ k_4^+}}, \end{aligned} \quad (\text{B18})$$

where a_i and c_i are the helicity and color indices of the final-state quarks, and D_{ij} are the conventional light-cone denominators (where the first subscript index $i = 1, 2$ refers to the first and second diagrams in Fig. 11, respectively, and the second index $j = 1, 2, 3$ numerates proper cuts shown with dashed vertical lines). Explicitly, these light-cone denominators are given by

$$D_{11} = -\frac{1}{2q^+} \left(\frac{\mathbf{k}_{2\perp}^2 + m_1^2}{\alpha_2} + \frac{(\mathbf{k}_{1\perp} + \ell)^2 + m_1^2}{\alpha_1 + z} \right) = -\frac{1}{2q^+} \frac{\mathbf{k}_{2\perp}^2 + m_1^2}{\alpha_2 \bar{\alpha}_2}, \quad (\text{B19})$$

$$D_{21} = -\frac{1}{2q^+} \left(\frac{\mathbf{k}_{1\perp}^2 + m_1^2}{\alpha_1} + \frac{(\mathbf{k}_{2\perp} + \ell)^2 + m_1^2}{\alpha_2 + z} \right) = -\frac{1}{2q^+} \frac{\mathbf{k}_{1\perp}^2 + m_1^2}{\alpha_1 \bar{\alpha}_1}, \quad (\text{B20})$$

$$D_{12} = D_{22} \equiv D_2 = -\frac{1}{2q^+} \left(\frac{\mathbf{k}_{1\perp}^2 + m_1^2}{\alpha_1} + \frac{\mathbf{k}_{2\perp}^2 + m_1^2}{\alpha_2} + \frac{\ell^2}{z} \right) \quad (\text{B21})$$

$$\begin{aligned} &= -\frac{1}{2q^+} \frac{\alpha_2 \bar{\alpha}_2 (\mathbf{k}_{1\perp} + \mathbf{k}_{2\perp} \frac{\alpha_1}{\bar{\alpha}_2})^2 + \frac{\alpha_1}{\bar{\alpha}_2} (1 - \alpha_1 - \alpha_2) \mathbf{k}_{2\perp}^2 + m_1^2 (\alpha_1 + \alpha_2) (1 - \alpha_1 - \alpha_2)}{\alpha_1 \alpha_2 (1 - \alpha_1 - \alpha_2)} \\ &= -\frac{1}{2q^+} \frac{\alpha_1 \bar{\alpha}_1 (\mathbf{k}_{2\perp} + \mathbf{k}_{1\perp} \frac{\alpha_2}{\bar{\alpha}_1})^2 + \frac{\alpha_2}{\bar{\alpha}_1} (1 - \alpha_1 - \alpha_2) \mathbf{k}_{1\perp}^2 + m_1^2 (\alpha_1 + \alpha_2) (1 - \alpha_1 - \alpha_2)}{\alpha_1 \alpha_2 (1 - \alpha_1 - \alpha_2)}, \end{aligned} \quad (\text{B22})$$

$$D_{13} = D_{23} = D_3 = -\frac{1}{2q^+} \left(\sum_{i=1}^2 \frac{\mathbf{k}_{i\perp}^2 + m_1^2}{2\alpha_i} + \sum_{i=3}^4 \frac{\mathbf{k}_{i\perp}^2 + m_2^2}{2\alpha_i} \right) \quad (\text{B23})$$

$$\begin{aligned} &= D_{12} - \frac{(\mathbf{k}_{3\perp} \alpha_4 - \mathbf{k}_{4\perp} \alpha_3)^2 + m_2^2 (\alpha_3 + \alpha_4)^2}{2q^+ \alpha_3 \alpha_4 (\alpha_3 + \alpha_4)} = D_{12} - \left(\frac{\alpha_3 + \alpha_4}{\alpha_3 \alpha_4} \right) \frac{q_{34}^2 + m_2^2}{2q^+}, \\ q_{34} &= \frac{\mathbf{k}_{3\perp} \alpha_4 - \mathbf{k}_{4\perp} \alpha_3}{\alpha_3 + \alpha_4}. \end{aligned} \quad (\text{B24})$$

To simplify the structure of Eqs. (B19)–(B23), we introduced the shorthand notation $\bar{\alpha}_i \equiv 1 - \alpha_i$, $i = 1 \dots 4$. The combination of momenta \mathbf{q}_{34} , defined in Eq. (B24), represents the relative motion momenta of quarks 3 and 4 (Fourier conjugate of a relative distance $\mathbf{r}_3 - \mathbf{r}_4$).

Technically, the structure of the denominators, up to trivial redefinitions, agrees with the findings of Ref. [109]. The expressions in the numerator of Eq. (B18) can be written out explicitly using the light-cone algebra from Refs. [16,107,109], yielding for the amplitude

$$\begin{aligned} \mathcal{A}_{c_1 c_2, c_3 c_4}^{a_1 a_2, a_3 a_4} = & \frac{1}{2\pi^2 (q^+)^2} \frac{e_q g^2 (t_a)_{c_1 c_2} \otimes (t_a)_{c_3 c_4}}{\sqrt{\alpha_1 \alpha_2} (1 - \alpha_1 - \alpha_2) (\alpha_3 + \alpha_4) D_2(\alpha_1, \mathbf{k}_1; \alpha_2, \mathbf{k}_2)} \\ & \times \left\{ \frac{1}{\mathbf{k}_{2\perp}^2 + m_1^2} \sqrt{\frac{\alpha_2}{\alpha_1}} \left[(\alpha_2 \delta_{\gamma, a_2} - \bar{\alpha}_2 \delta_{\gamma, -a_2}) \delta_{b, -a_2} \mathbf{k}_2 \cdot \boldsymbol{\varepsilon}_\gamma + \frac{m_q}{\sqrt{2}} \text{sign}(a_2) \delta_{\gamma, a_2} \delta_{b, a_2} \right] \right. \\ & \times \left[(\bar{\alpha}_2 \delta_{\lambda, a_1} + \alpha_1 \delta_{\lambda, -a_1}) \delta_{a_1, b} \mathbf{q}_1 \cdot \boldsymbol{\varepsilon}_\lambda^* + \frac{m_q (1 - \alpha_1 - \alpha_2)^2}{\sqrt{2} (1 - \alpha_2)} \text{sign}(-a_1) \delta_{\lambda, -a_1} \delta_{a_1, -b} \right] \\ & - \frac{1}{\mathbf{k}_{1\perp}^2 + m_1^2} \sqrt{\frac{\alpha_1}{\alpha_2}} \left[(\alpha_1 \delta_{\gamma, a_1} - \bar{\alpha}_1 \delta_{\gamma, -a_1}) \delta_{b, -a_1} \mathbf{k}_1 \cdot \boldsymbol{\varepsilon}_\gamma + \frac{m_q}{\sqrt{2}} \text{sign}(a_1) \delta_{\gamma, a_1} \delta_{a_1, b} \right] \\ & \times \left. \left[(\bar{\alpha}_1 \delta_{\lambda, a_2} + \alpha_2 \delta_{\lambda, -a_2}) \delta_{a_2, b} \mathbf{q}_2 \cdot \boldsymbol{\varepsilon}_\lambda^* + \frac{m_q (1 - \alpha_1 - \alpha_2)^2}{\sqrt{2} (1 - \alpha_1)} \text{sign}(-a_2) \delta_{\lambda, -a_2} \delta_{a_2, -b} \right] \right\} \\ & \times \frac{\frac{2(\alpha_3 + \alpha_4)}{\alpha_3 \alpha_4} \left[\left(\frac{\alpha_3}{\alpha_3 + \alpha_4} \delta_{\lambda, -a_3} - \frac{\alpha_4}{\alpha_3 + \alpha_4} \delta_{\lambda, a_3} \right) \delta_{a_3, -a_4} \mathbf{q}_{34} \cdot \boldsymbol{\varepsilon}_{-\lambda} + \frac{m_q}{\sqrt{2}} \text{sign}(a_3) \delta_{\lambda, a_3} \delta_{a_3, a_4} \right]}{D_2(\alpha_1, \mathbf{k}_1; \alpha_2, \mathbf{k}_2) - \frac{q_{34}^2 + m_2^2}{2q^+} \frac{(\alpha_3 + \alpha_4)}{\alpha_3 \alpha_4}}, \end{aligned} \quad (\text{B25})$$

where the momenta \mathbf{q}_i are defined as

$$\mathbf{q}_1 = -\left(\mathbf{k}_1 + \frac{\alpha_1}{1 - \alpha_2} \mathbf{k}_2 \right), \quad \mathbf{q}_2 = -\left(\mathbf{k}_2 + \frac{\alpha_2}{1 - \alpha_1} \mathbf{k}_1 \right). \quad (\text{B26})$$

We may observe that the amplitude (B25) is antisymmetric with respect to permutation of the momenta and helicities of the first two quarks, $(\alpha_1, \mathbf{k}_1, a_1) \leftrightarrow (\alpha_2, \mathbf{k}_2, a_2)$, and symmetric with respect to permutation of the momenta and helicities of the third and fourth quarks, $(\alpha_3, \mathbf{k}_3, a_3) \leftrightarrow (\alpha_4, \mathbf{k}_4, a_4)$. This symmetry simply reflects that the amplitude (B25) was evaluated as a sum of the left and right diagrams in Fig. 11, which can be related by charge conjugation. This symmetry allows to simplify some evaluations.

For evaluations in the dipole framework we need to rewrite the amplitude in configuration space, making a Fourier transformation over the transverse components,

$$\begin{aligned} \psi_{\bar{Q}Q\bar{Q}Q}^{(\gamma)}(\{\alpha_i, \mathbf{x}_i\}) = & \int \left(\prod_{i=1}^4 \frac{d^2 k_i}{(2\pi)^2} e^{i\mathbf{k}_i \cdot \mathbf{x}_i} \right) (2\pi)^2 \delta^2 \left(\sum \mathbf{k}_i \right) \\ & \times \mathcal{A}_{c_1 c_2, c_3 c_4}^{a_1 a_2, a_3 a_4}(\{\alpha_i, \mathbf{k}_i\}). \end{aligned} \quad (\text{B27})$$

In view of momentum conservation [Eq. (B4)], the wave function $\psi_{\bar{Q}Q\bar{Q}Q}^{(\gamma)}$ will be invariant with respect to global shifts,

$$\mathbf{x}_i \rightarrow \mathbf{x}_i + \mathbf{a}_i, \quad \mathbf{a}_i = \text{const}, \quad (\text{B28})$$

i.e., it should only depend on relative distances between quarks $|\mathbf{x}_i - \mathbf{x}_j|$. After straightforward evaluation of the integrals and algebraic simplifications, it is possible to reduce Eq. (B27) to the form

$$\psi_{\bar{Q}Q\bar{Q}Q}^{(\gamma)}(\{\alpha_i, \mathbf{x}_i\}) = A(\{\alpha_i, \mathbf{x}_i\}) + B(\{\alpha_i, \mathbf{x}_i\}), \quad (\text{B29})$$

where

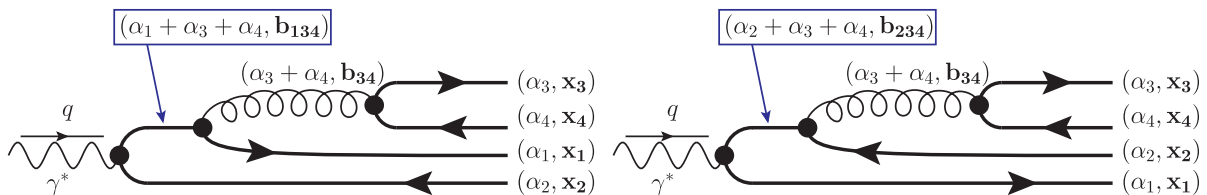


FIG. 12. Graphical illustration of the transverse momentum dependence of the wave function $\psi_{\gamma \rightarrow \bar{Q}Q\bar{Q}Q}(\{\alpha_i, \mathbf{r}_i\})$. The letters \mathbf{b}_{ij} and \mathbf{b}_{ijk} stand for the center-of-mass position of the partons ij and ijk . See the text for more details.

$$\begin{aligned}
A(\{\alpha_i, \mathbf{r}_i\}) = & -\frac{2e_q\alpha_s(m_Q)(t_a)_{c_1c_2} \otimes (t_a)_{c_3c_4}}{\pi^3(1-\alpha_1-\alpha_2)^2\sqrt{\alpha_1\alpha_2}} \int \frac{q_1 dq_1 k_2 dk_2}{\frac{\bar{\alpha}_2 q_1^2}{\alpha_1(1-\alpha_1-\alpha_2)} + \frac{m_1^2(\alpha_1+\alpha_2)}{\alpha_1\alpha_2} + \frac{k_2^2}{\alpha_2\bar{\alpha}_2}} \\
& \times \frac{1}{k_2^2 + m_1^2} \sqrt{\frac{\alpha_2}{\alpha_1}} [(\alpha_2\delta_{\gamma,a_2} - \bar{\alpha}_2\delta_{\gamma,-a_2})(\bar{\alpha}_2\delta_{\lambda,a_1} + \alpha_1\delta_{\lambda,-a_1})\delta_{a_1,-a_2} \\
& \times (\mathbf{n}_{2,134} \cdot \boldsymbol{\varepsilon}_\gamma)(\mathbf{n}_{1,34} \cdot \boldsymbol{\varepsilon}_\lambda^*) k_2 J_1(k_2|\mathbf{x}_2 - \mathbf{b}_{134}|) q_1 J_1(q_1|\mathbf{x}_1 - \mathbf{b}_{34}|) \\
& + \frac{m_q^2}{2} \delta_{\lambda,-a_1} \delta_{\gamma,a_2} \delta_{a_1,-a_2} J_0(k_2|\mathbf{x}_2 - \mathbf{b}_{134}|) J_0(q_1|\mathbf{x}_1 - \mathbf{b}_{34}|) \frac{(1-\alpha_1-\alpha_2)^2}{1-\alpha_2} \\
& - \frac{im_q}{\sqrt{2}} \text{sign}(a_2) \delta_{\gamma,a_2} \delta_{a_1,a_2} (\bar{\alpha}_2\delta_{\lambda,a_1} + \alpha_1\delta_{\lambda,-a_1}) \mathbf{n}_{1,34} \cdot \boldsymbol{\varepsilon}_\lambda^* q_1 J_1(q_1|\mathbf{x}_1 - \mathbf{b}_{34}|) J_0(k_2|\mathbf{x}_2 - \mathbf{b}_{134}|) \\
& - \frac{im_q}{\sqrt{2}} \text{sign}(a_1) \delta_{\lambda,-a_1} (\alpha_2\delta_{\gamma,a_2} - \bar{\alpha}_2\delta_{\gamma,-a_2}) \delta_{a_1,a_2} \frac{(1-\alpha_1-\alpha_2)^2}{1-\alpha_2} \\
& \times (\mathbf{n}_{2,134} \cdot \boldsymbol{\varepsilon}_\gamma) k_2 J_1(k_2|\mathbf{x}_2 - \mathbf{b}_{134}|) J_0(q_1|\mathbf{x}_1 - \mathbf{b}_{34}|)] \\
& \times \Psi_{a_3,a_4}^{-\lambda} \left(\frac{\alpha_3}{\alpha_3 + \alpha_4}, \mathbf{r}_{34}, m_2, \sqrt{m_2^2 + \frac{\alpha_3\alpha_4}{\alpha_3 + \alpha_4} \left[\frac{\bar{\alpha}_2 q_1^2}{\alpha_1(1-\alpha_1-\alpha_2)} + \frac{m_1^2(\alpha_1+\alpha_2)}{\alpha_1\alpha_2} + \frac{k_2^2}{\alpha_2\bar{\alpha}_2} \right]} \right) \quad (\text{B30})
\end{aligned}$$

and

$$B(\alpha_1, \mathbf{x}_1, \alpha_2, \mathbf{x}_2, \alpha_3, \mathbf{x}_3, \alpha_4, \mathbf{x}_4) = -A(\alpha_2, \mathbf{x}_2, \alpha_1, \mathbf{x}_1, \alpha_4, \mathbf{x}_4, \alpha_3, \mathbf{x}_3).$$

The variable $\mathbf{b}_{j_1 \dots j_n}$ corresponds to the position of the center of mass of n partons j_1, \dots, j_n and was defined earlier in Eq. (24). The variables $\mathbf{n}_{i,j_1 \dots j_n} = (\mathbf{x}_i - \mathbf{b}_{j_1 \dots j_n})/|\mathbf{x}_i - \mathbf{b}_{j_1 \dots j_n}|$ are unit vectors pointing from quark i towards the center of mass of a system of quarks $j_1 \dots j_n$. It is not possible to do the remaining integrals over q_1, k_2 analytically, nor present the wave function (B30) as a convolution of simpler “elementary” wave functions from Appendix B 1. Technically, this happens because in the language of traditional Feynman diagrams the intermediate (virtual) partons are off shell, and the integration over q_1, k_2 can be rewritten via integrals over virtualities of intermediate particles. Nevertheless, the structure of the coordinate dependence of $\psi_{\gamma \rightarrow \bar{Q}Q\bar{Q}Q}(\{\alpha_i, \mathbf{r}_i\})$ can still be understood using the simple rules suggested in Appendix B 1. Indeed, in the eikonal picture the transverse coordinates of all partons are frozen. The tree-like structure of the leading-order diagrams 1 and 2 in Fig. 11 and the iterative evaluation of the coordinate of the center of mass of two partons $\mathbf{b}_{ij} = (\alpha_i \mathbf{r}_i + \alpha_j \mathbf{r}_j)/(\alpha_i + \alpha_j)$ allow to reconstruct the transverse coordinates of all intermediate partons, as shown in Fig. 12. The variables $\mathbf{r}_1 - \mathbf{b}_{34}$ and $\mathbf{r}_2 - \mathbf{b}_{34}$ have the physical meaning of the relative distance between the recoil quark or antiquark and the emitted gluon. Similarly, the variables $\mathbf{r}_1 - \mathbf{b}_{234}$ and $\mathbf{r}_2 - \mathbf{b}_{134}$ can be interpreted as the size of the $\bar{Q}Q$ pair produced right after the splitting of the incident photon. These simple rules allow for the construction of the heavy $\bar{Q}Q\bar{Q}Q$ production amplitude in the gluonic field of the target.

The wave function $\psi_{\bar{Q}Q\bar{Q}Q}^{(\gamma)}(\{\alpha_i, \mathbf{r}_i\})$ has a few singularities which require special attention in order to guarantee that the amplitudes of the physical processes remain finite. For the meson pair production, the choice of the quarkonia wave functions (28)–(31), which vanish rapidly near the end points, is sufficient in order to guarantee the finiteness of the amplitudes (22)–(23).

b. Instantaneous contributions

According to canonical rules of the standard light-cone perturbation theory [16,107], the evaluations from the previous section should be supplemented by the instantaneous contributions of virtual partons, as show in the Figure 13. The propagators of the instantaneous off-shell quarks and gluons with momentum k are given by

$$S_{(\text{inst})}(k) = \frac{\gamma^+}{2k^+} \equiv \frac{(n \cdot \gamma)}{2(k \cdot n)}, \quad \Pi_{(\text{inst})}^{\mu\nu} = \frac{n_\mu n_\nu}{(k^+)^2}, \quad (\text{B31})$$

where n^μ is the light-cone vector in the minus direction. The results for the instantaneous contributions of gluons are quite straightforward to get, essentially repeating the evaluations from the previous subsection. Since $\gamma_+ \gamma_+ = 0$, there are no diagrams with two instantaneous propagators (quark and gluon) connected to the same vertex. The numerators of amplitudes with instantaneous propagators have a simple structure in view of the identities [16,107,109] $\bar{u}_{h_f}(p_1)\gamma_+ u_{h_i}(p_2) = 2\sqrt{p_1^+ p_2^+} \delta_{h_f, h_i}$ and $\bar{u}_h(p_1)\gamma_+ v_{\bar{h}}(p_2) = 2\sqrt{p_1^+ p_2^+} \delta_{h, -\bar{h}}$. The final result of the evaluation is

$$\psi_{\bar{Q}Q\bar{Q}Q}^{(\gamma)}(\{\alpha_i, \mathbf{r}_i\}) = A_g(\{\alpha_i, \mathbf{r}_i\}) + B_g(\{\alpha_i, \mathbf{r}_i\}) + A_q(\{\alpha_i, \mathbf{r}_i\}) + B_q(\{\alpha_i, \mathbf{r}_i\}), \quad (\text{B32})$$

where the subscript indices q, g on the right-hand side denote the parton propagator, which should be taken instantaneous (q for quark, g for gluon), and

$$\begin{aligned} A_g(\{\alpha_i, \mathbf{r}_i\}) = & -\frac{e_q \alpha_s(m_Q)(t_a)_{c_1 c_2} \otimes (t_a)_{c_3 c_4}}{\pi^4 (1 - \alpha_1 - \alpha_2)^3} \int q_1 dq_1 k_2 dk_2 J_0(q_1 |\mathbf{r}_1 - \mathbf{b}_{34}|) \\ & \times \frac{1}{\mathbf{k}_{2\perp}^2 + m_1^2} [(\alpha_2 \delta_{\gamma, a_1} - \bar{\alpha}_2 \delta_{a_1, -\gamma}) \delta_{a_1, -a_2} i \mathbf{n}_{2,134} \cdot \boldsymbol{\epsilon}_\gamma k_2 J_1(k_2 |\mathbf{r}_2 - \mathbf{b}_{134}|) \\ & + \frac{m_q}{\sqrt{2}} \text{sign}(a_1) \delta_{\gamma, a_1} \delta_{a_1, a_2} J_0(k_2 |\mathbf{r}_2 - \mathbf{b}_{134}|)] \alpha_3 \alpha_4 \delta_{a_3, -a_4} K_0(a_{34} \mathbf{r}_{34}), \end{aligned} \quad (\text{B33})$$

$$\begin{aligned} A_q(\{\alpha_i, \mathbf{r}_i\}) = & -\frac{e_q \alpha_s(m_q)(t_a)_{c_1 c_2} \otimes (t_a)_{c_3 c_4} \delta_{a_1, -a_2} \delta_{\gamma, -a_1}}{2\pi^4 (1 - \alpha_1 - \alpha_2)^2 \bar{\alpha}_2} \int q_1 dq_1 k_2 dk_2 \frac{J_0(q_1 |\mathbf{r}_1 - \mathbf{b}_{34}|) J_0(k_2 |\mathbf{r}_2 - \mathbf{b}_{134}|)}{D_2(\alpha_1, \mathbf{k}_1; \alpha_2, \mathbf{k}_2)} \\ & \times \left[-(\alpha_3 \delta_{-\gamma, a_3} - \alpha_4 \delta_{\gamma, a_3}) \delta_{a_3, -a_4} i \boldsymbol{\epsilon}_\gamma \cdot \mathbf{n}_{34} a_{34} K_1(a_{34} \mathbf{r}_{34}) - \frac{m_q (\alpha_3 + \alpha_4)}{\sqrt{2}} \text{sign}(a_3) \delta_{\gamma, -a_3} \delta_{a_3, a_4} K_0(a_{34} \mathbf{r}_{34}) \right], \end{aligned} \quad (\text{B34})$$

$$a_{34}(q_1, k_2) \equiv \sqrt{m_2^2 + \frac{\alpha_3 \alpha_4}{\alpha_3 + \alpha_4} \left[\frac{\bar{\alpha}_2 q_1^2}{\alpha_1 (1 - \alpha_1 - \alpha_2)} + \frac{m_1^2 (\alpha_1 + \alpha_2)}{\alpha_1 \alpha_2} + \frac{k_2^2}{\alpha_2 \bar{\alpha}_2} \right]}, \quad (\text{B35})$$

and the functions B_q, B_g can be obtained from A_q, A_g using

$$B_i(\alpha_1, \mathbf{x}_1, \alpha_2, \mathbf{x}_2, \alpha_3, \mathbf{x}_3, \alpha_4, \mathbf{x}_4) = -A_i(\alpha_2, \mathbf{x}_2, \alpha_1, \mathbf{x}_1, \alpha_4, \mathbf{x}_4, \alpha_3, \mathbf{x}_3), \quad i = q, g. \quad (\text{B36})$$

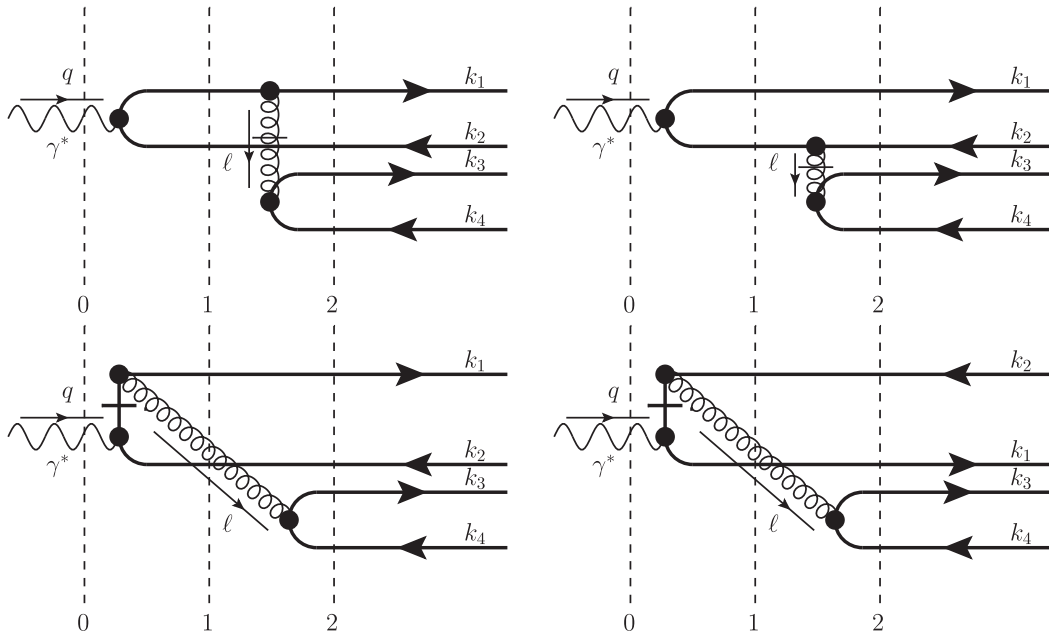


FIG. 13. Instantaneous contributions to the wave function $\psi_{\bar{Q}Q\bar{Q}Q}^{(\gamma)}$ defined in the text. The upper and lower rows correspond to instantaneous gluons and quarks, respectively. The vertical dashed lines denote light-cone denominators. The momenta k_i shown on the right-hand side are Fourier conjugates of the coordinates x_i . In what follows we will refer to the diagrams in the first row as A1, B1, and the diagrams in the second row as A2, B2, respectively.

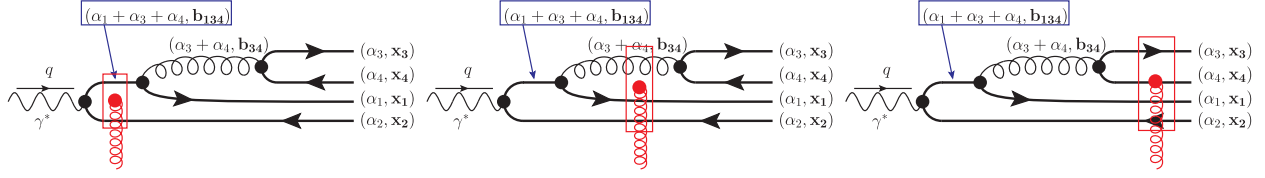


FIG. 14. Schematic illustration of the diagrams that contribute to a $\gamma \rightarrow \bar{Q}Q\bar{Q}Q$ subprocess, via single-gluon exchange in the t channel. For the sake of simplicity we omit a proton blob in the lower part. The square box with a gluon connected in the middle stands for the coupling of a dipole [sum of the couplings to all partons that pass through the block, $\sim \sum (\pm)\gamma(\mathbf{x}_i)t_a$]. The center of mass $\mathbf{b}_{i_1 \dots i_n}$ of a system of partons $i_1 \dots i_n$ is defined in Eq. (24). In all plots it the inclusion of diagrams that can be obtained by inversion of heavy quark lines is implied (“charge conjugation”).

APPENDIX C: SCATTERING AMPLITUDES IN THE EIKONAL APPROXIMATION

As discussed in Appendix A, in configuration space the interaction of the target with heavy quarks reduces to a mere multiplication by the factor $\pm\gamma(\mathbf{x}_\perp)$. For the evaluation of the scattering amplitude it is very instructive to use the light-cone evolution picture of the process, as shown in Fig. 11, tacitly assuming that the cuts (vertical dashed lines) in that figure separate different successive stages of the scattering process.

We start our discussion assuming that the interaction of high-energy partons with the target is dominated by single-gluon exchange. The colorless photon creates quark-anti-quark pair with transverse coordinates $(\mathbf{b}_{134}, \mathbf{x}_2)$ or $(\mathbf{x}_1, \mathbf{b}_{234})$, respectively, as shown in Fig. 14. The eikonal interaction can occur at any of the three stages of the process, so the Born amplitude of such a process includes a sum of contributions due to interactions at all stages,

$$\mathcal{A} = \mathcal{A}_1 + \mathcal{A}_2 + \mathcal{A}_3, \quad (\text{C1})$$

where the corresponding contributions $\mathcal{A}_{1,2,3}$ are given by

$$\mathcal{A}_1 = \psi_{\bar{Q}Q\bar{Q}Q}^{(\gamma)}(\alpha_1, \mathbf{x}_1; \alpha_2, \mathbf{x}_2; \alpha_3, \mathbf{x}_3; \alpha_4, \mathbf{x}_4; q) \sum_{acd} [\gamma_c(\mathbf{b}_{134}) - \gamma_c(\mathbf{x}_2)] \left(\frac{if_{acd} + d_{acd}}{2} \right) (t_d)_{c_1 c_2} (t_a)_{c_3 c_4} - (1 \leftrightarrow 2, 3 \leftrightarrow 4), \quad (\text{C2})$$

$$\begin{aligned} \mathcal{A}_2 = \psi_{\bar{Q}Q\bar{Q}Q}^{(\gamma)}(\alpha_1, \mathbf{x}_1; \alpha_2, \mathbf{x}_2; \alpha_3, \mathbf{x}_3; \alpha_4, \mathbf{x}_4; q) & \left\{ \sum_{acd} [\gamma_c(\mathbf{x}_1) + \gamma_c(\mathbf{x}_2) - 2\gamma_c(\mathbf{x}_{34})] \left(\frac{if_{acd}}{2} \right) (t_d)_{c_1 c_2} (t_a)_{c_3 c_4} \right. \\ & \left. + \sum_{acd} [\gamma_c(\mathbf{x}_1) - \gamma_c(\mathbf{x}_2)] \left(\frac{d_{acd}}{2} \right) (t_d)_{c_1 c_2} (t_a)_{c_3 c_4} + \sum_{acd} [\gamma_c(\mathbf{x}_1) - \gamma_c(\mathbf{x}_2)] \delta_{c_1 c_2} (t_c)_{c_3 c_4} \right\} - (1 \leftrightarrow 2, 3 \leftrightarrow 4), \quad (\text{C3}) \end{aligned}$$

$$\begin{aligned} \mathcal{A}_3 = \psi_{\bar{Q}Q\bar{Q}Q}^{(\gamma)}(\alpha_1, \mathbf{x}_1; \alpha_2, \mathbf{x}_2; \alpha_3, \mathbf{x}_3; \alpha_4, \mathbf{x}_4; q) & \left\{ \sum_{acd} [\gamma_c(\mathbf{x}_1) + \gamma_c(\mathbf{x}_2) - \gamma_c(\mathbf{x}_3) - \gamma_c(\mathbf{x}_4)] \left(\frac{if_{acd}}{2} \right) (t_d)_{c_1 c_2} (t_a)_{c_3 c_4} \right. \\ & \left. + \sum_{acd} [\gamma_c(\mathbf{x}_1) - \gamma_c(\mathbf{x}_2) + \gamma_c(\mathbf{x}_3) - \gamma_c(\mathbf{x}_4)] \left(\frac{d_{acd}}{2} \right) (t_d)_{c_1 c_2} (t_a)_{c_3 c_4} \right\} - (1 \leftrightarrow 2, 3 \leftrightarrow 4). \quad (\text{C4}) \end{aligned}$$

We may observe that all factors $\gamma_c(\mathbf{x}_i)$ always appear in the combination $\gamma_c(\mathbf{x}_i) - \gamma_c(\mathbf{x}_j)$, which guarantees that in the heavy quark mass limit, when the distances between the quarks are small, the corresponding amplitude is suppressed at least as $\sim 1/m_Q$. The three-gluon coupling $\sim\gamma(\mathbf{x}_{34})$ always appears in the combination $[\gamma_c(\mathbf{x}_1) + \gamma_c(\mathbf{x}_2) - 2\gamma_c(\mathbf{x}_{34})]$, in agreement with the earlier findings of Ref. [54].

For the case of two-gluon exchanges, we may repeat the same evaluations, taking into account the set of diagrams shown in Fig. 15. The final result of this evaluation is

$$\mathcal{A} = \psi_{\bar{Q}Q\bar{Q}Q}^{(\gamma)}(\alpha_1, \mathbf{x}_1; \alpha_2, \mathbf{x}_2; \alpha_3, \mathbf{x}_3; \alpha_4, \mathbf{x}_4; q) \quad (\text{C5})$$

$$\begin{aligned} & \times \{ \mathcal{C}_1 [(\gamma(\mathbf{x}_1) - \gamma(\mathbf{x}_4))^2 + (\gamma(\mathbf{x}_3) - \gamma(\mathbf{x}_2))^2] + 2\mathcal{C}_2 (\gamma(\mathbf{x}_1) - \gamma(\mathbf{x}_4)) (\gamma(\mathbf{x}_3) - \gamma(\mathbf{x}_2)) \\ & - + \mathcal{C}_3 (\gamma(\mathbf{x}_1) + \gamma(\mathbf{x}_2) - 2\gamma(\mathbf{x}_{34})) (\gamma(\mathbf{x}_1) + \gamma(\mathbf{x}_2) - \gamma(\mathbf{x}_3) - \gamma(\mathbf{x}_4)) \\ & + \mathcal{C}_1 (\gamma(\mathbf{b}_{134}) - \gamma(\mathbf{x}_2)) (\gamma(\mathbf{x}_3) - \gamma(\mathbf{x}_2)) + \mathcal{C}_2 (\gamma(\mathbf{b}_{134}) - \gamma(\mathbf{x}_2)) (\gamma(\mathbf{x}_1) - \gamma(\mathbf{x}_4)) \\ & + -\mathcal{C}_3 (\gamma(\mathbf{b}_{134}) - \gamma(\mathbf{x}_2)) (\gamma(\mathbf{x}_1) + \gamma(\mathbf{x}_2) - 2\gamma(\mathbf{x}_{34})) \\ & + \mathcal{C}_1 (\gamma(\mathbf{b}_{134}) - \gamma(\mathbf{x}_2))^2 + \mathcal{C}_4 (\gamma(\mathbf{x}_1) + \gamma(\mathbf{x}_2) - 2\gamma(\mathbf{x}_{34}))^2 \}, \quad (\text{C6}) \end{aligned}$$

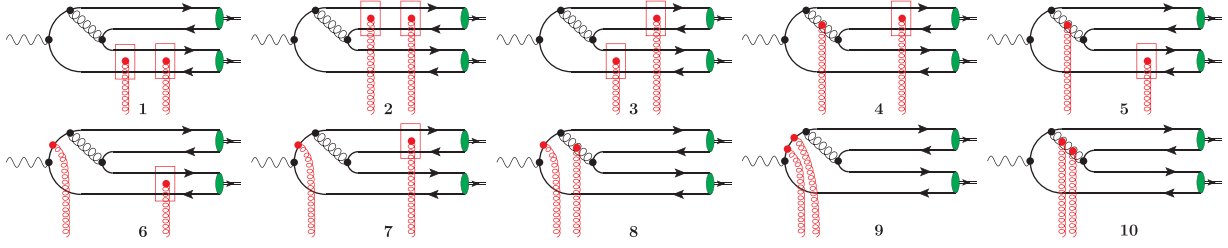


FIG. 15. Schematic illustration of the diagrams that contribute to meson pair production. For the sake of simplicity we approximate a Pomeron with a pair of t -channel gluons, and omit all possible gluon exchanges between them (as well as a proton blob in the lower part). The square box with a gluon connected in the middle stands for a dipole coupling [sum of the couplings of a quark and antiquark that pass through the block, $\sim(\gamma(\mathbf{x}_Q) - \gamma(\mathbf{x}_{\bar{Q}}))t_a$]. In all plots it the inclusion of diagrams that can be obtained by the inversion of the heavy quark lines is implied (“charge conjugation”).

where the color factors $\mathcal{C}_1 - \mathcal{C}_4$ were defined earlier in Sec. II B, in the text under Eq. (23). With the help of Eqs. (A5) and (A7), it is possible to rewrite the amplitude (C5) as

$$\begin{aligned}
\mathcal{A} = & \psi_{\bar{Q}Q\bar{Q}Q}^{(\gamma)}(\alpha_1, \mathbf{x}_1; \alpha_2, \mathbf{x}_2; \alpha_3, \mathbf{x}_3; \alpha_4, \mathbf{x}_4; q) \{ -2\mathcal{C}_1 [N(x, \mathbf{r}_{14}, \mathbf{b}_{14}) + N(x, \mathbf{r}_{23}, \mathbf{b}_{23})] \\
& + 2\mathcal{C}_2 [N(x, \mathbf{r}_{34}, \mathbf{b}_{34}) + N(x, \mathbf{r}_{12}, \mathbf{b}_{12}) - N(x, \mathbf{r}_{13}, \mathbf{b}_{13}) - N(x, \mathbf{r}_{24}, \mathbf{b}_{24})] \\
& + \mathcal{C}_3 [-2N(x, \mathbf{r}_{12}, \mathbf{b}_{12}) + N(x, \mathbf{r}_{13}, \mathbf{b}_{13}) + N(x, \mathbf{r}_{14}, \mathbf{b}_{14}) + N(x, \mathbf{r}_{23}, \mathbf{b}_{23}) + N(x, \mathbf{r}_{24}, \mathbf{b}_{24}) \\
& + 2N(x, \mathbf{r}_{1,34}, \mathbf{b}_{134}) + 2N(x, \mathbf{r}_{2,34}, \mathbf{b}_{234}) - 2N(x, \mathbf{r}_{3,34}, \mathbf{b}_{334}) - 2N(x, \mathbf{r}_{4,34}, \mathbf{b}_{344})] \\
& + \mathcal{C}_1 [N(x, \mathbf{r}_{2,134}, \mathbf{b}_{1234}) + N(x, \mathbf{r}_{23}, \mathbf{b}_{23}) - N(x, \mathbf{r}_{3,134}, \mathbf{b}_{1334})] \\
& + \mathcal{C}_2 [N(x, \mathbf{r}_{4,134}, \mathbf{b}_{1344}) + N(x, \mathbf{r}_{12}, \mathbf{b}_{12}) - N(x, \mathbf{r}_{1,134}, \mathbf{b}_{1,134}) - N(x, \mathbf{r}_{24}, \mathbf{b}_{24})] \\
& - \mathcal{C}_3 [-N(x, \mathbf{r}_{1,134}, \mathbf{b}_{1,134}) - N(x, \mathbf{r}_{2,134}, \mathbf{b}_{1234}) + N(x, \mathbf{r}_{12}, \mathbf{b}_{12}) \\
& + 2N(x, \mathbf{r}_{34,134}, \mathbf{b}_{34,134}) - 2N(x, \mathbf{r}_{2,34}, \mathbf{b}_{234})] + \mathcal{C}_1 N(x, \mathbf{r}_{2,134}, \mathbf{b}_{1234}) \\
& + \mathcal{C}_4 [2N(x, \mathbf{r}_{1,34}, \mathbf{b}_{134}) + 2N(x, \mathbf{r}_{2,34}, \mathbf{b}_{234}) - N(x, \mathbf{r}_{12}, \mathbf{b}_{12})] \}, \tag{C7}
\end{aligned}$$

where

$$\mathbf{r}_{1,34} = \mathbf{r}_1 - \frac{\alpha_3 \mathbf{r}_3 + \alpha_4 \mathbf{r}_4}{\alpha_3 + \alpha_4} = \frac{\alpha_3 \mathbf{r}_{13} + \alpha_4 \mathbf{r}_{14}}{\alpha_3 + \alpha_4}, \tag{C8}$$

$$\mathbf{r}_{2,34} = \frac{\alpha_3 \mathbf{r}_{23} + \alpha_4 \mathbf{r}_{24}}{\alpha_3 + \alpha_4}, \tag{C9}$$

$$\mathbf{r}_{3,34} = \frac{\alpha_4 \mathbf{r}_{34}}{\alpha_3 + \alpha_4}, \tag{C10}$$

$$\mathbf{r}_{4,34} = -\frac{\alpha_3 \mathbf{r}_{34}}{\alpha_3 + \alpha_4} = -\frac{\alpha_3}{\alpha_4} \mathbf{r}_{3,34}, \tag{C11}$$

$$\begin{aligned}
\mathbf{r}_{34,134} &= \frac{\alpha_3 \mathbf{r}_3 + \alpha_4 \mathbf{r}_4}{\alpha_3 + \alpha_4} - \frac{\alpha_1 \mathbf{r}_1 + \alpha_3 \mathbf{r}_3 + \alpha_4 \mathbf{r}_4}{\alpha_1 + \alpha_3 + \alpha_4} \\
&= -\frac{\alpha_1 (\alpha_3 \mathbf{r}_{13} + \alpha_4 \mathbf{r}_{14})}{(\alpha_3 + \alpha_4)(\alpha_1 + \alpha_3 + \alpha_4)}, \tag{C12}
\end{aligned}$$

$$\begin{aligned}
\mathbf{r}_{1,134} &= \mathbf{r}_1 - \frac{\alpha_1 \mathbf{r}_1 + \alpha_3 \mathbf{r}_3 + \alpha_4 \mathbf{r}_4}{1 - \alpha_2} \\
&= \frac{(1 - \alpha_2 - \alpha_3) \mathbf{r}_1 - \alpha_3 \mathbf{r}_3 - \alpha_4 \mathbf{r}_4}{1 - \alpha_2} = \frac{\alpha_3 \mathbf{r}_{13} + \alpha_4 \mathbf{r}_{14}}{1 - \alpha_2}, \tag{C13}
\end{aligned}$$

$$\begin{aligned}
\mathbf{r}_{2,134} &= \mathbf{r}_2 - \frac{\alpha_1 \mathbf{r}_1 + \alpha_3 \mathbf{r}_3 + \alpha_4 \mathbf{r}_4}{1 - \alpha_2} \\
&= \frac{(1 - \alpha_2) \mathbf{r}_2 - \alpha_3 \mathbf{r}_3 - \alpha_1 \mathbf{r}_1 - \alpha_4 \mathbf{r}_4}{1 - \alpha_2} \\
&= \frac{\alpha_1 \mathbf{r}_{21} + \alpha_3 \mathbf{r}_{23} + \alpha_4 \mathbf{r}_{24}}{1 - \alpha_2}, \tag{C14}
\end{aligned}$$

$$\begin{aligned}
\mathbf{r}_{3,134} &= \mathbf{r}_3 - \frac{\alpha_1 \mathbf{r}_1 + \alpha_3 \mathbf{r}_3 + \alpha_4 \mathbf{r}_4}{1 - \alpha_2} \\
&= \frac{(1 - \alpha_2 - \alpha_3) \mathbf{r}_3 - \alpha_1 \mathbf{r}_1 - \alpha_4 \mathbf{r}_4}{1 - \alpha_2} = \frac{\alpha_1 \mathbf{r}_{31} + \alpha_4 \mathbf{r}_{34}}{1 - \alpha_2}, \tag{C15}
\end{aligned}$$

$$\begin{aligned}
\mathbf{r}_{4,134} &= \mathbf{r}_4 - \frac{\alpha_1 \mathbf{r}_1 + \alpha_3 \mathbf{r}_3 + \alpha_4 \mathbf{r}_4}{1 - \alpha_2} \\
&= \frac{(1 - \alpha_2 - \alpha_4) \mathbf{r}_4 - \alpha_1 \mathbf{r}_1 - \alpha_3 \mathbf{r}_3}{1 - \alpha_2} = \frac{\alpha_1 \mathbf{r}_{41} + \alpha_3 \mathbf{r}_{43}}{1 - \alpha_2} \\
&= -\frac{\alpha_1 \mathbf{r}_{14} + \alpha_3 \mathbf{r}_{34}}{1 - \alpha_2}. \tag{C16}
\end{aligned}$$

If we introduce the variable $\mathbf{R} = \sum \alpha_i \mathbf{r}_i$, we may rewrite the above given expressions as

$$r_{1,134} = \mathbf{r}_1 - \frac{\mathbf{R} - \alpha_2 \mathbf{r}_2}{1 - \alpha_2} = \frac{\bar{\alpha}_2 \mathbf{r}_1 + \alpha_2 \mathbf{r}_2 - \mathbf{R}}{1 - \alpha_2}, \quad (\text{C17})$$

$$r_{2,134} = \mathbf{r}_2 - \frac{\mathbf{R} - \alpha_2 \mathbf{r}_2}{1 - \alpha_2} = \frac{\mathbf{r}_2 - \mathbf{R}}{1 - \alpha_2}, \quad (\text{C18})$$

$$r_{3,134} = \mathbf{r}_3 - \frac{\mathbf{R} - \alpha_2 \mathbf{r}_2}{1 - \alpha_2} = \frac{\bar{\alpha}_2 \mathbf{r}_3 + \alpha_2 \mathbf{r}_2 - \mathbf{R}}{1 - \alpha_2}, \quad (\text{C19})$$

$$r_{4,134} = \mathbf{r}_4 - \frac{\mathbf{R} - \alpha_2 \mathbf{r}_2}{1 - \alpha_2} = \frac{\bar{\alpha}_2 \mathbf{r}_4 + \alpha_2 \mathbf{r}_2 - \mathbf{R}}{1 - \alpha_2}. \quad (\text{C20})$$

Using the values of the color factors $\mathcal{C}_1 = (N_c^2 - 1)/4N_c = \mathcal{C}_2 + \mathcal{C}_3$, $\mathcal{C}_2 = -1/4N_c$, $\mathcal{C}_3 = N_c/4$, $\mathcal{C}_4 \equiv N_c/2 = 2\mathcal{C}_3$, and identifying the coefficient in front of $\psi_{\bar{Q}Q\bar{Q}Q}^{(\gamma)}$ in Eq. (C7) with $\sum_{\ell n} \sigma_\ell \sigma_n c_{\ell n} \gamma(\mathbf{b}_\ell) \gamma(\mathbf{b}_n)$ in Eq. (22), we get the final result (25). The evaluation of the amplitude (23) follows the same algorithm; technically, it is significantly simpler because the production of two colorless $\bar{Q}Q$ requires in this topology that each of the t -channel gluons should be attached to different quark loops, thus significantly reducing the number of possible diagrams. After straightforward algebraic simplifications, we can get the final result for this case, Eq. (26).

-
- [1] J. G. Korner and G. Thompson, *Phys. Lett. B* **264**, 185 (1991).
- [2] M. Neubert, *Phys. Rep.* **245**, 259 (1994).
- [3] G. T. Bodwin, E. Braaten, and G. P. Lepage, *Phys. Rev. D* **51**, 1125 (1995); **55**, 5853(E) (1997).
- [4] F. Maltoni, M. L. Mangano, and A. Petrelli, *Nucl. Phys. B* **519**, 361 (1998).
- [5] N. Brambilla, A. Vairo, and E. Mereghetti, *Phys. Rev. D* **79**, 074002 (2009); **83**, 079904(E) (2011).
- [6] Y. Feng, J. P. Lansberg, and J. X. Wang, *Eur. Phys. J. C* **75**, 313 (2015).
- [7] N. Brambilla *et al.*, *Eur. Phys. J. C* **71**, 1534 (2011).
- [8] P. L. Cho and A. K. Leibovich, *Phys. Rev. D* **53**, 6203 (1996).
- [9] P. L. Cho and A. K. Leibovich, *Phys. Rev. D* **53**, 150 (1996).
- [10] S. P. Baranov, *Phys. Rev. D* **66**, 114003 (2002).
- [11] S. P. Baranov and A. Szczurek, *Phys. Rev. D* **77**, 054016 (2008).
- [12] S. P. Baranov, A. V. Lipatov, and N. P. Zotov, *Phys. Rev. D* **85**, 014034 (2012).
- [13] S. P. Baranov and A. V. Lipatov, *Phys. Rev. D* **96**, 034019 (2017).
- [14] S. P. Baranov, A. V. Lipatov, and N. P. Zotov, *Eur. Phys. J. C* **75**, 455 (2015).
- [15] S. J. Brodsky, G. Kopp, and P. M. Zerwas, *Phys. Rev. Lett.* **58**, 443 (1987).
- [16] G. P. Lepage and S. J. Brodsky, *Phys. Rev. D* **22**, 2157 (1980).
- [17] C. Berger and W. Wagner, *Phys. Rep.* **146**, 1 (1987).
- [18] M. S. Baek, S. Y. Choi, and H. S. Song, *Phys. Rev. D* **50**, 4363 (1994).
- [19] Y. Bai, S. Lu, and J. Osborne, *Phys. Lett. B* **798**, 134930 (2019).
- [20] W. Heupel, G. Eichmann, and C. S. Fischer, *Phys. Lett. B* **718**, 545 (2012).
- [21] R. J. Lloyd and J. P. Vary, *Phys. Rev. D* **70**, 014009 (2004).
- [22] J. Vijande, N. Barnea, and A. Valcarce, *Int. J. Mod. Phys. A* **22**, 561 (2007).
- [23] J. Vijande, A. Valcarce, and J.-M. Richard, *Few Body Syst.* **54**, 1015 (2013).
- [24] X. Chen, *Phys. Rev. D* **100**, 094009 (2019).
- [25] A. Esposito and A. D. Polosa, *Eur. Phys. J. C* **78**, 782 (2018).
- [26] R. Cardinale (LHCb Collaboration), *Proc. Sci., LHCP2018* (2018) 191.
- [27] R. Aaij *et al.* (LHCb Collaboration), *J. High Energy Phys.* **10** (2018) 86.
- [28] L. Capriotti (LHCb Collaboration), *J. Phys. Conf. Ser.* **1137**, 012004 (2019).
- [29] R. Aaij *et al.* (LHCb), *Sci. Bull.* **65**, 1983 (2020).
- [30] V. P. Goncalves, B. D. Moreira, and F. S. Navarra, *Eur. Phys. J. C* **76**, 103 (2016).
- [31] V. P. Goncalves and R. Palota da Silva, *Phys. Rev. D* **101**, 034025 (2020).
- [32] V. P. Goncalves and M. V. T. Machado, *Eur. Phys. J. C* **49**, 675 (2007).
- [33] S. Baranov, A. Cisek, M. Klusek-Gawenda, W. Schafer, and A. Szczurek, *Eur. Phys. J. C* **73**, 2335 (2013).
- [34] H. Yang, Z. Q. Chen, and C. F. Qiao, *Eur. Phys. J. C* **80**, 806 (2020).
- [35] V. P. Goncalves, B. D. Moreira, and F. S. Navarra, *Eur. Phys. J. C* **76**, 388 (2016).
- [36] S. Bhattacharya, A. Metz, V. K. Ojha, J. Y. Tsai, and J. Zhou, *arXiv:1802.10550*.
- [37] A. Accardi *et al.*, *Eur. Phys. J. A* **52**, 268 (2016).
- [38] Press release at the website of the United States Department of Energy: <https://www.energy.gov/articles/us-department-energy-selects-brookhaven-national-laboratory-host-major-new-nuclear-physics>.
- [39] Press-release at the website of the Brookhaven National Laboratory (BNL): <https://www.bnl.gov/newsroom/news.php?a=116998>.
- [40] R. Abdul Khalek *et al.*, *arXiv:2103.05419*.
- [41] J. L. Abelleira Fernandez *et al.* (LHeC Study Group), *J. Phys. G* **39**, 075001 (2012).
- [42] M. Mangano, CERN yellow reports: Monographs, Vol. **3** (2017), 10.23731/CYRM-2017-003.

- [43] P. Agostini *et al.* (LHeC and FCC-he Study Group), *J. Phys. G* **48**, 110501 (2021).
- [44] A. Abada *et al.* (FCC Collaboration), *Eur. Phys. J. C* **79**, 474 (2019).
- [45] CEPC Study Group, [arXiv:1809.00285](https://arxiv.org/abs/1809.00285).
- [46] J. B. Guimarães da Costa *et al.* (CEPC Study Group), [arXiv:1811.10545](https://arxiv.org/abs/1811.10545).
- [47] L. V. Gribov, E. M. Levin, and M. G. Ryskin, *Phys. Rep.* **100**, 1 (1983).
- [48] L. D. McLerran and R. Venugopalan, *Phys. Rev. D* **49**, 2233 (1994).
- [49] L. D. McLerran and R. Venugopalan, *Phys. Rev. D* **49**, 3352 (1994).
- [50] L. D. McLerran and R. Venugopalan, *Phys. Rev. D* **50**, 2225 (1994).
- [51] A. H. Mueller and J. Qiu, *Nucl. Phys.* **B268**, 427 (1986).
- [52] L. McLerran and R. Venugopalan, *Phys. Rev. D* **49**, 3352 (1994); **50**, 2225 (1994); **59**, 094002 (1999).
- [53] K. J. Golec-Biernat and M. Wusthoff, *Phys. Rev. D* **60**, 114023 (1999).
- [54] B. Z. Kopeliovich and A. V. Tarasov, *Nucl. Phys.* **A710**, 180 (2002).
- [55] B. Kopeliovich, A. Tarasov, and J. Hufner, *Nucl. Phys.* **A696**, 669 (2001).
- [56] N. N. Nikolaev and B. G. Zakharov, *J. Exp. Theor. Phys.* **78**, 598 (1994), <https://inspirehep.net/literature/383552>.
- [57] Y. V. Kovchegov, *Phys. Rev. D* **60**, 034008 (1999).
- [58] Y. V. Kovchegov and H. Weigert, *Nucl. Phys.* **A784**, 188 (2007).
- [59] I. Balitsky and G. A. Chirilli, *Phys. Rev. D* **77**, 014019 (2008).
- [60] Y. V. Kovchegov and E. Levin, *Camb. Monogr. Part. Phys., Nucl. Phys., Cosmol.* **33**, 1 (2012).
- [61] I. Balitsky, *Phys. Lett. B* **518**, 235 (2001).
- [62] F. Cougoulic and Y. V. Kovchegov, *Phys. Rev. D* **100**, 114020 (2019).
- [63] C. A. Aidala *et al.*, [arXiv:2002.12333](https://arxiv.org/abs/2002.12333).
- [64] Y. Q. Ma and R. Venugopalan, *Phys. Rev. Lett.* **113**, 192301 (2014).
- [65] B. Lehmann-Dronke, P. V. Pobylitsa, M. V. Polyakov, A. Schafer, and K. Goeke, *Phys. Lett. B* **475**, 147 (2000).
- [66] B. Lehmann-Dronke, A. Schafer, M. V. Polyakov, and K. Goeke, *Phys. Rev. D* **63**, 114001 (2001).
- [67] B. Clerbaux and M. V. Polyakov, *Nucl. Phys.* **A679**, 185 (2000).
- [68] M. Diehl, T. Gousset, and B. Pire, [arXiv:hep-ph/9909445](https://arxiv.org/abs/hep-ph/9909445).
- [69] J. Breitweg *et al.* (ZEUS Collaboration), *Eur. Phys. J. C* **6**, 603 (1999).
- [70] X. D. Ji and J. Osborne, *Phys. Rev. D* **58**, 094018 (1998).
- [71] J. C. Collins and A. Freund, *Phys. Rev. D* **59**, 074009 (1999).
- [72] D. Mueller, D. Robaschik, B. Geyer, F. M. Dittes, and J. Horejsi, *Fortschr. Phys.* **42**, 101 (1994).
- [73] X. D. Ji, *Phys. Rev. D* **55**, 7114 (1997).
- [74] X. D. Ji, *J. Phys. G* **24**, 1181 (1998).
- [75] A. V. Radyushkin, *Phys. Lett. B* **380**, 417 (1996).
- [76] A. V. Radyushkin, *Phys. Rev. D* **56**, 5524 (1997).
- [77] A. V. Radyushkin, Generalized parton distributions, *At The Frontier of Particle Physics* (2001), pp. 1037–1099, [10.1142/9789812810458_0027](https://arxiv.org/abs/10.1142/9789812810458_0027).
- [78] J. C. Collins, L. Frankfurt, and M. Strikman, *Phys. Rev. D* **56**, 2982 (1997).
- [79] S. J. Brodsky, L. Frankfurt, J. F. Gunion, A. H. Mueller, and M. Strikman, *Phys. Rev. D* **50**, 3134 (1994).
- [80] K. Goeke, M. V. Polyakov, and M. Vanderhaeghen, *Prog. Part. Nucl. Phys.* **47**, 401 (2001).
- [81] M. Diehl, T. Feldmann, R. Jakob, and P. Kroll, *Nucl. Phys.* **B596**, 33 (2001); **B605**, 647(E) (2001).
- [82] A. V. Belitsky, D. Mueller, and A. Kirchner, *Nucl. Phys.* **B629**, 323 (2002).
- [83] M. Diehl, *Phys. Rep.* **388**, 41 (2003).
- [84] A. V. Belitsky and A. V. Radyushkin, *Phys. Rep.* **418**, 1 (2005).
- [85] V. Kubarovsky (CLAS Collaboration), *Nucl. Phys. B, Proc. Suppl.* **219–220**, 118 (2011).
- [86] R. Dupré, M. Guidal, S. Niccolai, and M. Vanderhaeghen, *Eur. Phys. J. A* **53**, 171 (2017).
- [87] P. A. M. Guichon and M. Vanderhaeghen, *Prog. Part. Nucl. Phys.* **41**, 125 (1998).
- [88] W. K. Tung, S. Kretzer, and C. Schmidt, *J. Phys. G* **28**, 983 (2002).
- [89] H. Kowalski, L. Motyka, and G. Watt, *Phys. Rev. D* **74**, 074016 (2006).
- [90] H. Kowalski and D. Teaney, *Phys. Rev. D* **68**, 114005 (2003).
- [91] A. H. Rezaeian, M. Siddikov, M. Van de Klundert, and R. Venugopalan, *Phys. Rev. D* **87**, 034002 (2013).
- [92] S. Chekanov *et al.* (ZEUS Collaboration), *Nucl. Phys.* **B695**, 3 (2004).
- [93] A. Aktas *et al.* (H1 Collaboration), *Eur. Phys. J. C* **46**, 585 (2006).
- [94] V. M. Budnev, I. F. Ginzburg, G. V. Meledin, and V. G. Serbo, *Phys. Rep.* **15**, 181 (1975).
- [95] Y. Hatta, E. Iancu, K. Itakura, and L. McLerran, *Nucl. Phys.* **A760**, 172 (2005).
- [96] H. G. Dosch, T. Gousset, G. Kulzinger, and H. J. Pirner, *Phys. Rev. D* **55**, 2602 (1997).
- [97] J. Nemchik, N. N. Nikolaev, and B. G. Zakharov, *Phys. Lett. B* **341**, 228 (1994); J. Nemchik, N. N. Nikolaev, E. Predazzi, and B. G. Zakharov, *Z. Phys. C* **75**, 71 (1997); J. R. Forshaw, R. Sandapen, and G. Shaw, *Phys. Rev. D* **69**, 094013 (2004).
- [98] S. J. Brodsky, T. Huang, and G. P. Lepage, *Proceedings of the Banff Summer Institute on Particles and Fields, held at the Banff Center in Banff, Alberta, Canada, 1981*. Published as a standalone “Particles and Fields”, edited by A. Z. Capri and A. N. Kamal (Plenum Publishing Corporation, New York, 1983), ISBN: 978-1-4613-3595-5, 10.1007/978-1-4613-3593-1.
- [99] S. J. Brodsky, J. R. Hiller, D. S. Hwang, and V. A. Karmanov, *Phys. Rev. D* **69**, 076001 (2004).
- [100] M. V. Terentev, *Sov. J. Nucl. Phys.* **24**, 106 (1976), <https://inspirehep.net/literature/109844>.
- [101] A. Stadler, S. Leitão, M. T. Peña, and E. P. Biernat, *Few Body Syst.* **59**, 32 (2018).
- [102] D. Daniel, R. Gupta, and D. G. Richards, *Phys. Rev. D* **43**, 3715 (1991).
- [103] T. Kawanai and S. Sasaki, *Phys. Rev. Lett.* **107**, 091601 (2011).
- [104] T. Kawanai and S. Sasaki, *Phys. Rev. D* **89**, 054507 (2014).

- [105] A. H. Rezaeian and I. Schmidt, *Phys. Rev. D* **88**, 074016 (2013).
- [106] E. Iancu and A. H. Mueller, *Nucl. Phys.* **A730**, 460 (2004).
- [107] S. J. Brodsky, H. C. Pauli, and S. S. Pinsky, *Phys. Rep.* **301**, 299 (1998).
- [108] J. D. Bjorken, J. B. Kogut, and D. E. Soper, *Phys. Rev. D* **3**, 1382 (1971).
- [109] T. Lappi and R. Paatelainen, *Ann. Phys. (Amsterdam)* **379**, 34 (2017).
- [110] J. Bartels, K. J. Golec-Biernat, and K. Peters, *Acta Phys. Pol. B* **34**, 3051 (2003), <https://inspirehep.net/literature/612076>.
- [111] H. Hänninen, T. Lappi, and R. Paatelainen, *Ann. Phys. (Amsterdam)* **393**, 358 (2018).